Titania minerals of Upper Jurassic- Lower Cretaceous sandstones of the Scotian Basin

By

Alexis Imperial

A Thesis Submitted to
Saint Mary's University, Halifax, Nova Scotia
In Partial Fulfillment of the Requirements for
the Degree of Master of Science in Applied Science.

April 2022, Halifax, Nova Scotia

Approved: Dr. Georgia Pe-Piper
Supervisor

Approved: Dr. David J.W. Piper
Committee Member

Approved: Dr. Jason Clyburne
Committee Member

Approved: Dr. Mark Deptuck
External Examiner

Date: April 21st 2022

Abstract

Titania minerals of Upper Jurassic- Lower Cretaceous sandstones of the Scotian Basin

By Alexis Imperial

A study of titania (TiO_2) minerals was performed to test the hypothesis that precipitation of late diagenetic titania minerals in reservoir sandstones of the Scotian Basin is related to the migration of hydrocarbons. Reservoir sandstones of Upper Jurassic- Lower Cretaceous from the Scotian Basin showed all three polymorphs of titania to be present as authigenic minerals indicating Titanium (Ti) was mobile. Diagenetic anatase and brookite are more prominent than diagenetic rutile. Anatase is mostly early diagenetic, whereas brookite is usually late diagenetic and is abundant in reservoir sandstones above the free-water level. The availability and mobility of Ti is attributed to the dissolution of Ti-containing minerals (ilmenite, pseudorutile, biotite) enhanced by Ti complexes formed from hydrocarbon-rich and highly saline fluids. This study suggests that the precipitation of diagenetic brookite may be due to the incorporation of Fe and V during hydrocarbon charge and the presence of Cl^- in the circulating fluids, which favour brookite polymorph formation.

April 21st 2022

Acknowledgements

I would like to thank my supervisor Dr. Georgia Pe-Piper for providing me advice and guidance throughout the research process. The completion of this study could not have been possible without her constant support and patience. I am very thankful for everything she taught me and I am honoured to have her as a mentor.

I would also like to thank my committee members for sharing their knowledge that helped refine this thesis. Thank you to Dr. David J.W. Piper for all his valuable critiques, comments and recommendations. His insights and suggestions greatly contributed to the completion of this thesis. Thank you to Dr. Jason Clyburne for providing alternative perspective and for always having encouraging words.

Lastly, thank you to Randolph Corney, Xiang Yang, Mitch Kerr and Dan Macdonald for their assistance with sample preparation, sample analysis and technical support.

This work was funded by a grant from Nova Scotia Offshore Energy Research Association (OERA) to Dr. Georgia Pe-Piper.

Table of Contents

List of figures

List of tables

List of appendices

Chapter 1: Introduction

1.1 Purpose and objectives of the study

The main purpose of this study is to investigate if titania (TiO_2) minerals can be used as a tool to track hydrocarbon migration and accumulation in petroleum sedimentary basins. In this study, titania is used as a term to collectively group polymorphs of TiO_2: rutile, anatase and brookite. Although Titanium (Ti) is commonly regarded as an immobile element, widespread late diagenetic titania minerals have been observed from the Late Jurassic–Early Cretaceous reservoir sandstones of the Scotian Basin, offshore Nova Scotia, eastern Canada (Pe-Piper et al. 2011). The Scotian Basin is an active petroleum system and has been an important source of oil and gas (Fig. 1). Furthermore, recent studies in Ti- mobility have suggested that Ti can be mobilized in the presence of organic acids produced during maturation of hydrocarbons (Parnell et al. 2004; Schulz et al. 2016; Liu et al. 2019). These observations suggest that late diagenesis of titania minerals may be useful in understanding basin reservoir quality. Although the diagenesis of the Late Jurassic-Early Cretaceous sandstones in the Scotian basin has been well studied, the processes of Ti-migration and the precipitation of late diagenetic authigenic titania remains poorly understood. Knowledge of the relationship between titania minerals and hydrocarbon generation can provide better understanding of petroleum generation, migration and accumulation, and can therefore help discover potential hydrocarbon reservoirs in the area.

Frequently, titania minerals are found with other Ti- rich minerals (e.g. ilmenite, pseudorutile, kleberite). Pseudorutile (Fe_2Ti_3O) and kleberite ($FeTi_6O_{11}(OH)_5$) are

intermediate minerals found during alteration of ilmenite ($FeTiO_3$) to rutile (TiO_2) (Teuffer and Temple 1966; Grey et al. 2013). A quick mineral identification can be difficult at times as these minerals can share similar petrographic and chemical characteristics. Therefore, in addition to the initial purpose of the study, Raman spectra of pseudorutile and kleberite were investigated in order to determine a simpler way of identifying these minerals. This new method will be able to immediately distinguish these two minerals from titania minerals and other Ti-rich minerals.

The main objectives of this study are thus: (i) determine conditions under which Ti is mobile in reservoir sandstones, (ii) understand the controls that affect the precipitation of diagenetic titania minerals, (iii) establish a correlation between titania and hydrocarbons, and (iv) identify a characteristic Raman spectrum for pseudorutile and kleberite. In this way, this research aims to answers questions like: (a) is the precipitation of diagenetic titania minerals controlled by burial depth, secondary porosity, amount and type of porosity, and overpressure and (b) what is the role of high salinity and the presence of hydrocarbon fluids in the precipitation of late diagenetic titania minerals?

1.2. Thesis organisation

This thesis consists of seven chapters. Chapter 1 introduces the purpose and objectives of the thesis. Chapter 2 discusses the geological setting of the Scotian Basin, previous studies on Ti-mobility, titania minerals and pseudorutile. Chapter 3 thoroughly describes the selected samples and outlines procedures and techniques used for the thesis.

The main body of this thesis is discussed in chapter 4 and 5. Both chapters were prepared as separate manuscripts for journal publication and therefore may include some repetition. In chapter 4, diagenetic titania minerals: rutile, anatase, brookite, were investigated to determine if the formation of a specific polymorph of titania is related in any way to hydrocarbon generation and migration in the Scotian Basin. This study proposes an updated paragenetic sequence of authigenic titania minerals for the Upper Jurassic- Lower Cretaceous sandstones and a new model for Ti transport and titania mineral precipitation during hydrocarbon charge.

Chapter 5 investigates the Raman spectra of pseudorutile and kleberite to determine an alternative way of identifying these minerals. This study reveals that both minerals can easily be identified using Laser Raman spectroscopy. It is proposed that the identified spectra be used to easily distinguish pseudorutile and kleberite.

Chapter 6 summarizes the most important issues discussed in Chapter 4 and 5. Chapter 7 completes the thesis with a list of significant findings and conclusions. In addition, supplementary data, figures and tables are organised as appendices at the end of the thesis.

Chapter 2: Literature Review

2.1. Geological Setting

The Scotian Basin is a passive continental margin basin offshore Nova Scotia in the central North Atlantic Ocean (Fig. 1a), formed as a result of Late Triassic rifting and seafloor spreading that began in the Early or Middle Jurassic (Wade and MacLean, 1990). The late Jurassic uplift of the Labrador Rift and reactivation of major strike-slip faults in the Appalachians led to the uplift of the crystalline basement and supplied large amounts of clastic sediments, deposited predominantly as deltaic sandstones and shales (Pe-Piper and Piper, 2004; Zhang et al. 2014). Jurassic rocks are principally carbonates, including the Upper Jurassic Abenaki Formation carbonate bank in the western part of the basin and mixed limestones and clastic rocks of the Mic Mac Formation in the eastern part of the basin. Upper Jurassic to Lower Cretaceous rocks comprise fluvial, deltaic, and shelf sandstones and shales of the Mississauga and Logan Canyon Formations (Fig. 1b).

Salt tectonics highly controlled the deposition of sediments in the Scotian Basin. Late Triassic- Early Jurassic Argo salt formation is one of the first sediments to be deposited in the tectonic subbasin of the Scotian Basin (Fig. 1b) (Barss et al. 1979). During the Late Jurassic- Early Cretaceous, the Argo Salt Formation was remobilized causing regional extensional deformation on the outer shelf and upper slope, resulting in normal faults and regional subsidence (Kendell, 2012). Accommodation of thick and narrow successions of prodeltaic sandstones accumulated beneath the Scotian Shelf, (Cummings and Arnott 2005). Deltaic and shoreface sandstones of are the primary source

of Upper Jurassic- Lower Cretaceous gas and lesser oil in the Scotian Basin (Fig. 1b) (Wade and MacLean, 1990).

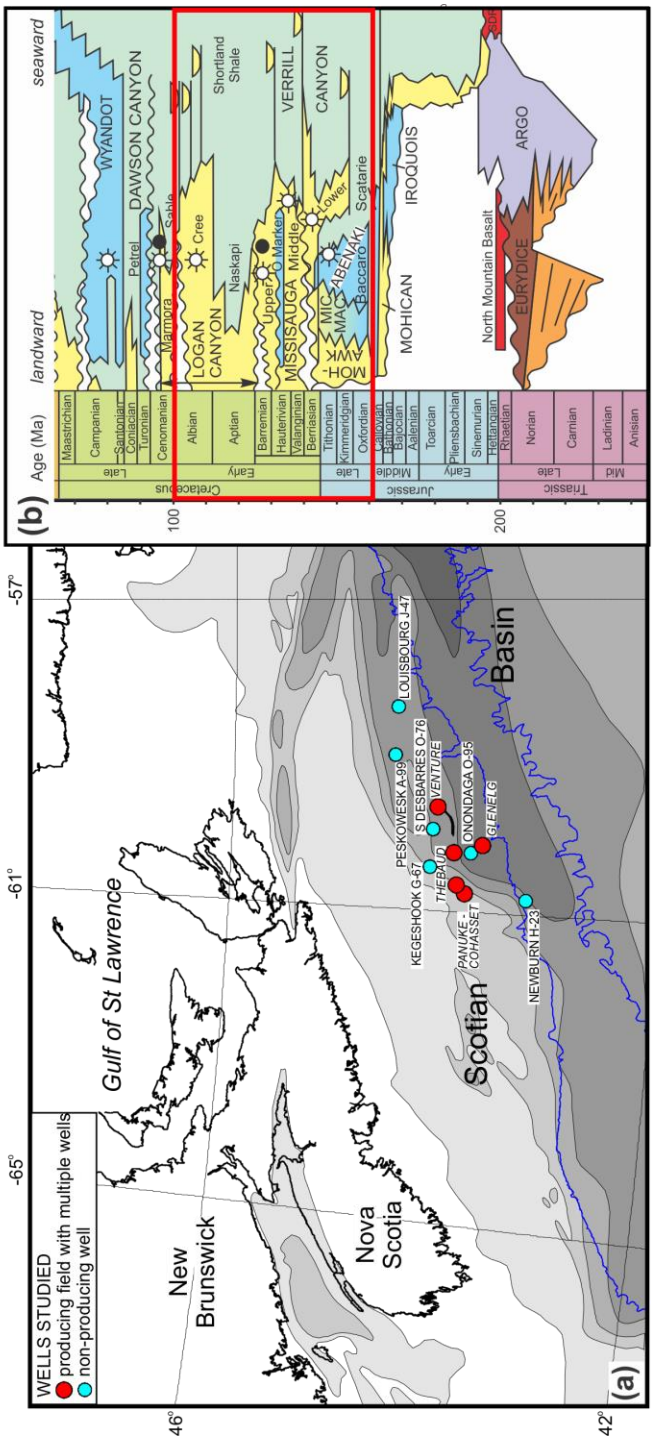

Figure 1. (a) Map of the Scotian Basin showing location of studied wells and fields (Base map modified from Wade and MacLean, 1990). Red dots show oil and/or gas producing fields (Paunke-Cohasset, Glenelg, Thebaud, and Venture) with multiple wells and blue dots show surrounding non-producing wells (Newburn H-23, Kegeshook G-67, Onondaga O-95, South Desbarres O-76, Peskowesk A-99, Louisburg J-47). **(b)** Stratigraphic column of the Mesozoic rocks of the Scotian Basin (Modified from Weston et al. 2012).

2.2. Titania minerals and Ti-mobility

Generally, titania is a high temperature and high pressure mineral usually occurring in metamorphic rocks (greenschist to eclogite) (Meinhold 2010). Under lower temperatures, titania has been observed to precipitate under controlled laboratory environments. In chemistry, titania is often used as a catalyst and therefore numerous studies have been performed into determining which phase of titania precipitate under various controlled laboratory environments.

Rutile is the most common and most stable titania phase at any given temperature. The ideal temperature for rutile is >900 °C (Allen et al. 2018). Studies have also shown that rutile precipitation requires very low pH (acidic conditions) and favors non-complexing ions (Pottier et al. 2001). In other cases, doping of Fluorine (F) ions favors rutile formation (Trapalis et al. 2008).

Anatase is metastable and precipitates at temperatures of 100-500 °C, and as the temperature increases, anatase formation also increases. The ideal temperature for anatase is 600 °C (Allen et al. 2018). Anatase also forms under high pH conditions (pH >9.0 precipitates pure anatase) and similar to rutile, Fluorine doping causes an increase in anatase formation (Li et al. 2007, Schulz et al. 2016). However, Fluorine favors anatase more than rutile. The crystallinity of anatase improves upon Fluorine doping and prevents formation of brookite crystals and also prevents anatase to rutile transformation (Trapalis et al. 2008). In other studies, Sulphate (SO^{2-}_4) ions also favor anatase precipitation (Pottier et al. 2001, Li et al. 2007).

Brookite is metastable and similar to anatase precipitates at temperatures of 100-500 °C. The ideal temperature for brookite is 100 °C and brookite formation decreases as the temperature increases (Allen et al. 2018). Brookite favors low to intermediate pH conditions (Li et al. 2007, Schulz et al. 2016) and most studies proposed that Chloride (Cl) ions are necessary for brookite formations (Pottier et al. 2001, Li et al. 2007, Schulz et al. 2016).

Although commonly regarded as immobile, recent studies of Titanium in nature, specifically in soils and black shales, suggest that Ti can be mobilized by the presence of organic acids (Parnell et al. 2004, Schulz et al. 2016, Liu et al. 2019) and that large amounts of Ti can be dissolved in fluids rich in organic acids (Schulz et al. 2016, Parnell et al. 2017). In addition, the generation of hydrocarbon liquids can lead to complete destruction of Ti-bearing minerals and initiate Ti mobilization due to the formation of organic-Ti complexes (Liu et al. 2019).

2.3. Titania minerals in the Scotian Basin

Diagenesis of titania minerals in the Scotian Basin was previously studied by Pe-Piper et al. (2011). The authors documented two occurrences of authigenic titania minerals, during (eogenesis) early diagenesis and (mesogenesis) late diagenesis. Eodiagenetic titania replaces non-compacted detrital fragments of plant material (phytodetritus) and as concentric layers fill intergranular pore spaces bounded by quartz grains lacking overgrowths, and is associated with eodiagenetic kaolinite. Mesodiagenetic titania has a lower P content and is associated with secondary porosity or

occurs in flattened phytodetritus. Ti is facilitated by the presence of meteoric waters that contain humic acids at lowstand boundaries during eodiagenesis, whereas Ti mobility during mesodiagenesis is due to the release of organic acids during the early stages of hydrocarbon generation.

The availability of Ti in the Scotian Basin is attributed to the abundant supply of Ti-bearing detrital minerals. In many basins, Ti is supplied principally in titanomagnetite, ilmenite, biotite and amphibole (Morad and AlDahan, 1986; Liu et al., 2019). Ti in the Scotian Basin was supplied by rivers, principally from detrital grains of ilmenite and their alteration products (Pe-Piper et al. 2005). Detrital titania minerals observed by Ledger (2014) in the Scotian Basin, often show signs of dissolution or partial dissolution and are present with an abundance of up to 3% by volume (Pe-Piper et al. 2011). In addition, the shales of the Scotian Basin have an unusually abundant supply of Ti (1 wt% Ti), double that of global average shales (Pe-Piper et al., 2008).

Chapter 3: Materials and Methods

3.1. Materials

Polished thin sections of core samples were chosen from wells previously studied for fluid inclusion and diagenesis. The selected samples reflect a wide range of burial depths and stratigraphic levels within the Upper Jurrasic- Lower Creataceous sandstones of the Scotian Basin with a focus on hydrocarbon producing wells (Fig. 2; Table 1). The samples from conventional cores were provided by the Canada-Nova Scotia Offshore Petroleum Board (CNSOPB) Geoscience Research Centre and polished thin sections were made from these samples by Vancouver Petrographics Ltd.

Samples of pseudorutile and kleberite grains from Neptune Island (South Australia) and Indonesia were provided by the Commonwealth Scientific and Industrial Research Organisation (CSIRO), Division of Mineral Resources, Australia. The loose grains were mounted and made into three separate 1-inch epoxy pucks, one for each locality. The pucks were made by placing compression mounting compound powder in a Buehler SimpliMet 1000™ automatic mounting press with a 3-minute bake time at 180 °C and 2100 psi, and an 11-minute cool down. The grains were carefully placed on top of the powder before pressing. The pucks were then polished using diamond paste and were studied under transmitted and reflected light microscope. Five grains with a smooth and flat surface from each sample locality were chosen for this study.

Table 1. Summary table of studied samples.

						% diagenetic titania			plug	
Well and depth	Lithostrat	Facies	Seq. Stratigraphy or depositional environment	Reservoir sand	# of analysed grains	Rutile	Anatase	Brookite	Permeability	Porosity
Glenelg E-58										
E-58 3443.86	UM	9	HST-RST	Sand B	19	3	14	83	0.02	7.4
E-58 3524.00	UM	0	HST-RST	Sand C1	12	3	42	55	0.33	13.4
E-58 3526.28	UM	9	HST-RST	Sand C1	17	8	33	59	19.6	18.3
E-58 3530.30	UM	9	HST-RST	Sand C1	39	2	24	74	0.9	11.2
E-58 3532.19	UM	3	WRS	Sand C1	5	7	56	37	0.01	8.9
E-58 3538.24	UM	9	HST-RST	Sand C1	18	11	15	74	15.9	18.5
E-58 3552.15	UM	9	HST-RST	Sand C1	11	0	75	25	0.04	9.5
E-58 3710.80	UM	0	HST-RST		22	17	57	26	0.09	10.8
Venture field										
Venture B-52										
B-52 4708.62	LM	2			20	3	70	27	0.01	3.4
B-52 4940.55	LM	4	tidal-estuarine[1]		25	2	8	90	5.37	15.3
B-52 4954.36	LM	4	SB-tidal estuarine[2]	Sand 6u	12	3	8	89	3.97	15.2
B-52 5045.32	LM	4	tidal-estuarine[1]	Sand 7	19	3	71	26	0.22	4.7
B-52 5047.51	LM	4	tidal-estuarine[1]	Sand 7	6	0	100	0	0.23	7
B-52 5119.97	LM	4	tidal-estuarine[1]		19	10	29	61	12.2	15.5
Venture H-22										
H-22 4909.12	LM	0	tidal-estuarine	Sand 5	11	9	9	82		
H-22 4957.21	LM	9	SDDF-PDM		7	21	71	9	0.49	13.4
H-22 5028.32	LM	4	SDDF-PDM	Sand 7	17	18	71	11	0.56	16.3
Venture B-13										
B-13 4701.20	LM	3			13	17	83	0	0.013	4.1
B-13 4965.27	LM	9	SDDF-PDM		25	20	77	3	0.11	15.1
V4 5383.28-5383.54	LM	9			14	36	21	43		

Thebaud field										
Thebaud I-93										
I-93 3080.26	MM	4			18	19	31	50	689	20.3
I-93 3925.79	LM	4		Sand A	4	25	0	75	7.26	11.8
I-93 3950.18	LM	2		Sand A	15	24	71	6	0.1	0.5
Thebaud #3										
Th#3 3917.60	LM	4		Sand A	29	0	0	100	852	21.7
Th#3 4424.62	LM	1&2		Sand F1	18	0	11	89	1.51	11.3
TH#3 4426.97	LM	1&2		Sand F1	7	10	32	58	0.07	8.7
Thebaud #5										
Th#5 4624.15	LM	2		Sand E2	18	15	35	50	0.11	9.3
Th#5 4925.84	LM	4			22	14	14	73	65.7	19.7
Th#5 4936.34	LM	4		Sand F3	8	10	19	71	1.84	13.4
Cohasset field										
Cohasset A-52										
A-52 2145.11	MC	3			10	19	44	38	0.34	21.3
A-52 2230.38	MC	4			27	3	48	48	0.01	4.7
A-52 2388.02	LC	9			1	0	0	100	10240	22.7
A-52 2436.83	LC	9			30	35	65	0	149	25.4
A-52 2440.04	LC	9			16	5	79	16	0.01	5.9
Panuke field										
Panuke B-90										
B-90 2221.92	NS	0			24	14	35	51	9.96	0.223
B-90 2303.75A	UM	3			11	23	26	51	0.88	13.2
B-90 2303.75B	UM	3			6	21	28	51	0.88	13.2
B-90 2393.92	UM	4			5	7	20	73	0.04	3.1
Other wells										
Peskowesk A-99										
A-99 2209.83	LC	4			3	0	0	100		
A-99 2221.17	LC	0			5	0	0	100		
A-99 2231.82	LC	4x			2	0	0	100		
A-99 2249.39	LC	4x			4	50	50	0		
A-99 2945.38	MM	0			25	0	12	84		

Kegeshook G-67										
G-67 1907.39	LC	4			14	50	14	36	386	29.1
G-67 2113.39	UM	9			2	100	0	0	32.6	20.7
Newburn H-23										
H-23 4913.80	UM	?0	fine sandstones		8	63	24	13		
H-23 5213.50	MM	?0	fine sandstones		21	57	43	0		
H-23 5408.50	MM	?0	fine sandstones		10	40	0	60		
Louisbourg J-47										
J-47 4528.05	MM	4x			17	18	0	82		
J-47 5445.94	MM	10s			10	30	50	20		
South Debarres O-76										
O-76 3809.60	LM	9g			22	18	23	59		
O-76 5952.65	MM	9g			8	37	13	50		
Onondaga O-95										
O-95 3266.71	MM	4o			12	17	83	0	0.04	4.6
O-95 3269.82	MM	4o			14	20	50	10	0.03	2

Footnotes with abbreviations and sources: HST-RST = high stand and regressive systems tracts. Facies from Gould et al. (2012). Plug and porosity from Zhang et al. (2015). MC = middle Cree, LC = lower Cree, NS = Naskapi, UM = upper Missisauga, MM = middle Missisauga, LM = lower Missisauga, MicMac = Mic Mac.

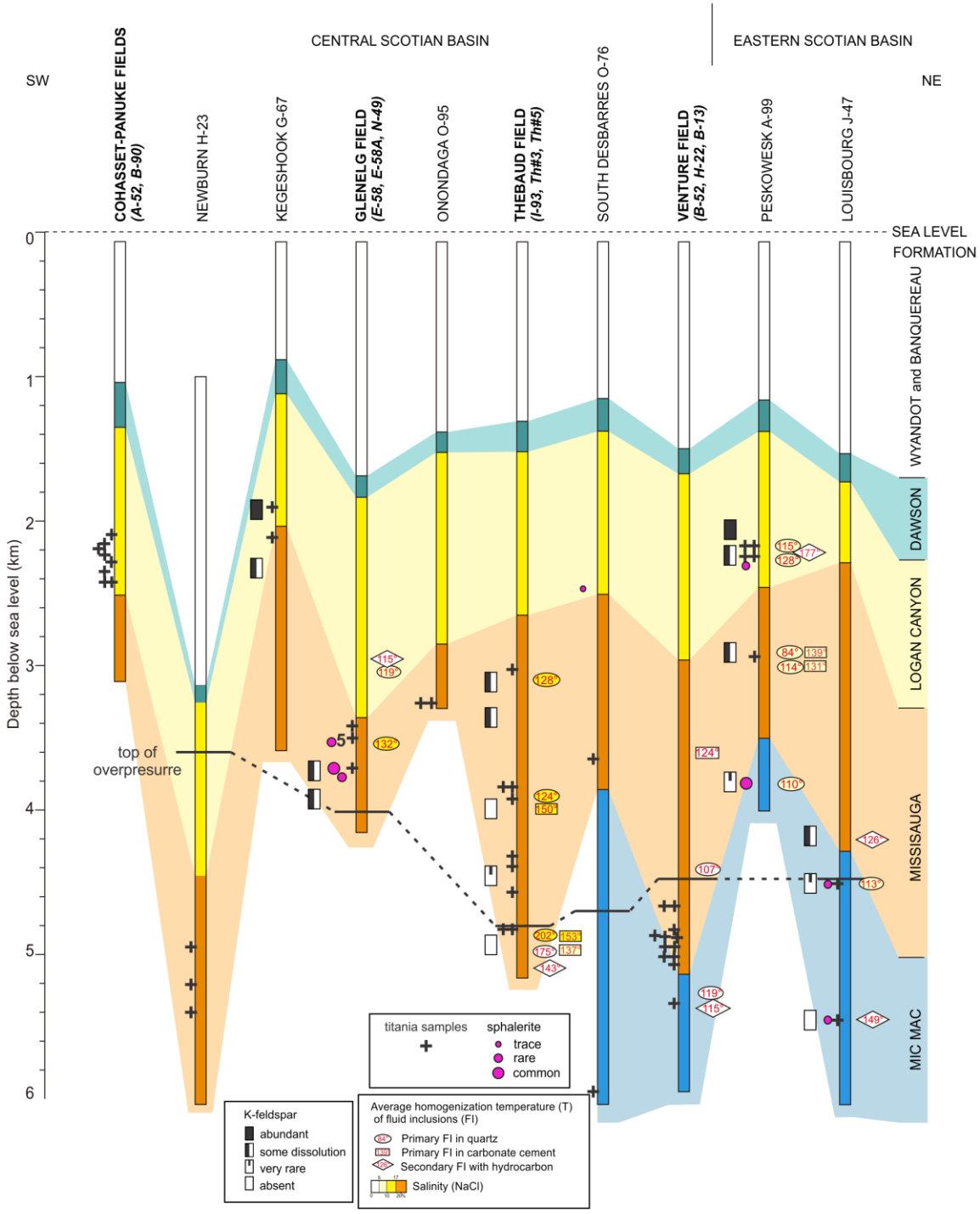

Figure 2. Stratigraphic sections of studied wells.

3.2. Analytical techniques

The selected sandstone samples were studied using various analytical techniques. At first, a petrographic microscope with polarized and reflected light was used to identify titania minerals, pseudorutile and kleberite. Such a microscope was also used to study mineral morphology and textures in order to be able to distinguished detrital titania from diagenetic titania minerals. The samples were then analysed using: (1) Scanning electron microscope (SEM) for chemical mineral analyses, mineral identification and textural relationships; (2) Electron microprobe (EMP) for quantitative chemical analyses and; (3) Laser Raman spectroscopy for crystal structure determination. Mineral abbreviations used in this thesis are after Whitney and Evans, 2010.

3.2.1. Scanning Electron Microscope (SEM)

Minerals in the samples were analysed by electron dispersion spectroscopy (EDS) using a scanning electron microscope. SEM analyses were acquired for mineral identification and to distinguish chemical composition of detrital and diagenetic titania minerals. The Oxford Instrument's INCA program was used as an X-ray data acquisition software for all EDS analyses. Back-scattered electron (BSE) images were obtain to describe mineral morphology and textural relationships.

SEM analysis was performed in the Regional Analytical Centre at Saint Mary's University using a TESCAN MIRA 3 LMU Variable Pressure Schottky Field Emission Scanning Microscope. The SEM is equipped with both a backscattered electron detector

(BSE) and an INCA X-max 80mm^2 Silicon Drift Detector (SDD) Energy Dispersive Spectrometer which are able to provide qualitative elemental/phase information and semiquantitative elemental information respectively about the sample being analyzed. The EDS system has a detection limit of < 0.1%. A pure cobalt plate was used as a standard to calibrate the beam for analysis. The beam has an average diameter of approximately <10 nm and has an X-ray production volume of ~10 μm (depending on the minerals). The SEM has a maximum resolution of 1.2 nm at 30kV. All analyses were acquired using a power of 20kV.

3.2.2. Electron Microprobe (EMP)

Diagenetic titania minerals, pseudorutile and kleberite were analysed using an electron microprobe for quantitative chemical analyses. Electron microprobe mineral analyses were acquired at the Regional Electron Microprobe Centre at Dalhousie University, in Halifax. The analysis was performed using a JEOL-8200 electron microprobe (EMP) which is equipped with a Noran 133 eV dispersive spectrometer and five wavelength spectrometers. The EMP is also equipped with a wavelength dispersive spectrometer (WDS) and gives more accurate chemical analyses for further precision. The instrument was operated at 15 kV and the same set of standards were chosen for all analysed minerals. FeO content from pseudorutile and kleberite from electron microprobe chemical analyses were recalculated as Fe_2O_3 and a H_2O content of 3.2 was added, based on the chemical analyses of pseudorutile and kleberite of Grey et al. (2013).

3.2.3. Laser Raman Spectroscopy

Laser Raman spectroscopy was used to differentiate titania minerals: rutile, anatase and brookite, and to identify a characteristic Raman spectrum for both pseudorutile and kleberite. Raman spectroscopy was performed at the Regional Analytical Centre at Saint Mary's University using a Horiba Jobin-Yvon LabRam HR confocal instrument. The instrument uses a 100 mW 532 nm Nd-YAG diode laser from Toptica Phonotics and a Synapse charge-coupled device form Horiba Jobin-Yvon. It uses a maximum of 100x Olympus MPlanN objective for image capture and analysis.

Analyses were acquired using a 25 μm confocal hole diameter, and 600 grooves/mm grating was used for all analyses, yielding a spectral resolution of approximately ±2 cm. Spectra were collected using an accumulation of three twelve-second acquisitions with a laser spot size of approximately 1 μm at 50% laser power. The spectra were collected in two spectral windows 200–4000 cm^{-1} and 200–2600 cm^{-1}. Analysed samples had carbon coating removed using methanol to increase the intensity of the peaks and to ensure more accurate results.

3.3. Stratigraphic setting of the studied wells

Sandstone stratigraphy and lithofacies in the Scotian Basin have been studied extensively (eg. Cummings et al. 2006; Karim et al. 2008, 2010; Gould et al. 2011). For this project, various samples from wells throughout the central Scotian Basin were selected. In addition, samples from four oil and gas producing fields were also selected. The most recently updated stratigraphic correlations and sediment lithofacies

classifications of Karim et al. (2008, 2010) and Gould et al. (2011) were mainly used in this study. Listed below are the common facies present in all studied wells. Their depositional environment is shown in parentheses:

Lithofacies 0 – mudstone with sandstone and siltstone beds and laminae (prodeltaic seaward of river mouth/ prodeltaic turbidites).

Lithofacies 1 – bioturbated mudstone (shelf).

Lithofacies 2 – fine sandstone, mudstone (shoreface and open shelf).

Lithofacies 3 – conglomerate formed with bioturbated shelly sandy mudstone to muddy sandstone generally with some coarse sand or granule sized intraclasts and/or lithic clasts. Commonly sideritic diagenesis or are bioclastic and oolitic limestones (transgressive marine sediment).

Lithofacies 4 – fine to coarse sandstone, interbedded mudstone with siltstone laminae (fluvial to tidal estuary).

Lithofacies 5 – fine to medium sandstones with minor mudstone (sandy tidal flats)

Lithofacies 9 – thick bedded sandstones in graded beds (river mouth to prodelta turbidite).

A more detailed sequence stratigraphy of the Venture, Thebaud, Glenelg, and Cohasset-Panuke fields producing fields is discussed below. A brief summary of the stratigraphy of the other wells is also presented.

3.3.1. Venture field

The Upper Jurassic- Lower Cretaceous sandstones of the Venture field is located in a deep rollover anticline developed on normal listric growth fault. Gas reservoirs were determined in the Lower member of the Mississauga Formation between 4406 and 5101 m in depth. Additional reservoirs in the deeper strata are overpressured. Cummings and Arnott (2005) established a detailed lithofacies description and their model consists primarily of two main units: (a) channel-form units of strongly tide-influenced estuarine fill of incised valleys and (b) upward-coarsening units of storm-dominated delta front sandstones, prodeltaic mudstone and shelf carbonates. Gould et al. (2010) redefined the lithofacies arguing that the delta front sandstones of Cummings and Arnott (2005) were actually of delta-front turbidite origin. Karim et al. (2008, 2010) found similar facies at both the Glenelg and Thebaud fields.

Sampled intervals:

Venture B-52: 4708.62 m, 49401.55 m, 4954.36 m, 5045.32 m, 5047.51 m and 5119.97 m. *Venture H-22*: 4909.12 m, 4957.21 m, 5028.32 m. *Venture B-13*: 4965.27 m

3.3.2. Thebaud field

The Thebaud field is situated near the western edge of the Sable Delta complex. Similar to Venture field, Thebaud is located in a rollover anticline structure, bounded by two large east-west listric growth faults. Wells in the Thebaud field were correlated by Karim et al. (2008) using gamma log data and lithostratigraphic picks. Gamma signals were acquired from the Offshore Petroleum Board and lithostratigraphic picks were from

Hughes and Baker (1999) for Thebaud #3 and #5, and from Maclean and Wade (1993) for Thebaud I-93. Five conventional cores were taken from the Thebaud I-93 well. Cores 1 and 2 are above the overpressure zone, located in the Middle Member of the Mississauga Formation. Cores 3, 4 and 5 are overpressured, located in the Lower Member of the Mississauga Formation.

Sampled intervals:

Thebaud I-93: 3080.26 m, 3950.18 m, 4925.84 m. *Thebaud* 3: 3917.60 m, 4426.97 m. *Thebuad* 5: 4624.15 m.

3.3.3. Glenelg field

The Glenelg field is also located within a rollover anticline separated by growth faults, similar to Venture and Thebaud fields. Karim et al. (2008) correlated and established a sequence stratigraphy of the Mississauga Formation using important surface boundaries defined and correlated by Cummings and Arnott (2005) using gamma signals. Gas pools in several wells in the Glenelg field were defined by CNSOPB (2000). Glenelg N-49 has gas pools B, C-1 and D. Glenelg E-58A has gas pool E and Glenelg J-48 has gas pool G.

Sampled intervals:

Glenelg E-58: 3524.00 m, 3526.28 m, 3530.30 m, 3538.24 m, 3552.15 m. *Glenelg H-49*: 3443.86 m.

3.3.4. Cohasset-Panuke fields

The Cohasset-Panuke field includes the Como P-21, Panuke B-90, Cohasset A-52, Balmoral M-32 and Lawrence D-14 wells. The wells are located on the western side of Sable Island in the Sable Subbasin. Gould et al. (2012) established a lateral correlation within the Panuke-Cohasset area in the upper part of the Mississauga Formation and the Cree Member of the Logan Canyon Formation using gamma log data and sediment facies. Reservoir sandstones were located at the top of the Mississauga Formation; P2 and P3 sandstones.

Sampled intervals:

Samples were chosen from Panuke B-90 well and Cohasset A-52 well. *Panuke B-90* well with depth intervals: 2221.92 m, 2303.75 m, 2393.92 m. *Cohasset A-52* well with depth intervals: 2145.11 m, 2330.38 m, 2436.83 m, 2440.04 m.

3.3.5. Surrounding wells

Samples were also studied from Newburn H-23, Kegeshook G-67, Onondaga O-95, South Desbarres O-76, Peskowesk A-99 and Louisbourg J-47. Kegeshook G-67, South Desbarres O-79 and Peskowesk A-99 are considered dry wells. Newburn H-23 is part of the Nova Scotia Deepwater Drilling Project and is currently considered a dry well, although several thin (2-3m) gas-bearing sands were encountered (CNSOPB 2002). Onondaga O-95 recovered gas at 3265.02 m depth (CNSOPB 2012) and Loiusbourg J-47 contain mainly gas-prone (Type IIB-III and III) source beds deposited on an open marine

shelf (Mukhopadhyay and Wade 1990). These surrounding wells will be referred to as "wet wells".

Sampled intervals:

Peskowesk A-99: 2209.83 m, 2221.17 m, 2231.82 m, 2249.49 m, 2945.38 m. *Kegeshook G-67*: G-67 1907.39 m, 2113.39 m. *Newburn H-23*: 4913.80 m, 5213.50 m, 5408.50 m. *Louisbourg J-47*: 4528.05 m, 5445.94 m. *South Desbarres O-76*: 38.09.60 m, 5952.65 m. *Onondaga O-95*: 3266.71 m, 3269.82 m.

Chapter 4: The use of titania polymorphs as indicator of mesodiagenesis during hydrocarbon charge

Abstract

Authigenic Titania (TiO_2) minerals were observed in the Upper Jurassic- Lower Cretaceous reservoir sandstones of the Scotian Basin, suggesting Titanium (Ti) was mobile in the system. Although diagenetic rutile is rare, relatively large amounts of diagenetic anatase and brookite are present. Anatase is mostly early diagenetic whereas brookite is usually late diagenetic and is abundant in reservoir sandstones above the free-water level. The availability and mobility of Ti is attributed to the dissolution of Ti-bearing minerals enhanced by Ti complexes formed from hydrocarbon-rich and highly saline fluids. This study suggests that the precipitation of diagenetic brookite may be due to the incorporation of Fe and V during hydrocarbon charge and the presence of Cl^- in fluids, which favour the formation of brookite.

4.1. Introduction

Titanium (Ti) is widely accepted as an immobile element during diagenesis and therefore titania (TiO_2) minerals are often considered to be of detrital origin. However recent studies have shown that Ti can be mobilized under very acidic conditions and enhanced in the presence of hydrocarbon-rich fluids (Parnell et al. 2004; Pe-Piper et al. 2011; Schulz et al. 2016; Liu et al. 2019). Organic acids released during generation of hydrocarbons can lead to complete dissolution of Ti-bearing minerals and prompt Ti mobilization due to chelation of Ti^{4+} in organic complexes (Parnell et al. 2004; Fuchs et

al. 2015; Liu et al. 2019). An earlier study of titania minerals from pro-deltaic Cretaceous sandstones of the Scotian Basin recognized the prevalence of authigenic titania during both eodiagenesis and mesodiagenesis (Pe-Piper et al. 2011). The authors suggested that Ti mobility during early diagenesis was facilitated by humic acids in meteoric waters released at sea level lowstands, whereas precipitation of late diagenetic titania minerals might be associated with petroleum generation during hydrocarbon charge. However, the specific mechanisms of titania polymorph precipitation and Ti-migration during hydrocarbon charge remains unknown.

The Scotian Basin is an active petroleum sedimentary basin located offshore Nova Scotia, in eastern Canada (Fig. 1a). Thick salt (halite) accumulated in the basin during the late Triassic rifting before initial spreading in the central Atlantic Ocean (Wade and MacLean 1990). The abundant salt produced saline formation waters to circulate in the basin. The combination of high heat flow in the Mid Cretaceous (Karim et al., 2012, Bowman et al, 2012) and saline formation waters resulted in the precipitation of late diagenetic minerals such as: sphalerite, barite and hydrothermal zircon, which co-occur with diagenetic titania (Pe-Piper et al. 2015; 2017).

Studies of titania authigenesis in the presence of hydrocarbons have mostly focused on organic-rich soil and black shales (Fuchs et al. 2015; Schulz et al. 2016; Liu et al. 2019). Anatase is the dominant titania phase mineral to precipitate with bitumen and/or at oil-water contacts in shales and siltstones (Fuchs et al. 2015; Schulz et al. 2016; Liu et al. 2019), whereas brookite has been reported in bitumen-bearing basement reservoir rock (Parnell et al. 2019). Laboratory syntheses of nano-crystalline TiO_2 solids

showed that pH, initial grain size, temperature and available ligands control the precipitation and transformation of titania phases (Pottier 2001; Arboil et al. 2002; Yu et al. 2002; Li et al. 2007; Zhang and Banfield, 2014). In natural systems, growth and stability of titania polymorphs is mainly controlled by local pH conditions (Zhang and Banfield, 2014).

The main objective of this study is to determine if titania polymorphs can be used as a tool in tracking hydrocarbon migration in petroleum sedimentary basins. This has been achieved by understanding the overall regional and stratigraphical occurrence and abundance of titania polymorphs in the Scotian Basin. The chemical composition, timing and distribution of the diagenetic titania polymorphs relative to other diagenetic minerals further constrains the overall paragenetic evolution of the basin, and thus illustrates the relationship between titania minerals, hydrocarbon charge and fluid conditions in the basin.

4.2. Geological Setting

The Scotian Basin (Fig. 1a) is a passive continental margin basin offshore Nova Scotia, in the central North Atlantic Ocean. The basin formed as a result of Late Triassic rifting and seafloor spreading that began in the Early or Middle Jurassic (Wade and MacLean, 1990). The late Jurassic uplift of the Labrador Rift and reactivation of major strike-slip faults in the Appalachians led to the uplift of the crystalline basement and supplied large amounts of clastic sediments, predominantly sandstones and shales, in the Scotian Basin in the Early Cretaceous (Pe-Piper and Piper, 2004; Zhang et al. 2014).

Jurassic carbonate rocks are prevalent in the western part of the basin forming the Abenaki Formation, while Jurassic carbonates mixed with clastic rocks dominate the eastern part forming the Mic Mac Formation. Upper Jurassic to Lower Cretaceous sandstones and shales of fluvial, deltaic, and shelf origin formed the Mississauga and Logan Canyon Formations. Upper Cretaceous and Cenozoic rocks are mostly shale intermixed with marl and pelagic carbonates of the Dawson Canyon, Wyandot and Banquereau formations (Fig. 1b).

Abundant accumulation of salt in the basin's history produced widespread salt-related deformation (salt tectonics), contributing to the circulation of saline formation waters. The Argo Formation was remobilized mainly in the Jurassic and Cretaceous as a result of loading by shelf deltas (Kendell, 2012), which produced widespread salt expulsion creating accommodation of thick and narrow successions of pro-deltaic sandstones beneath the Scotian Shelf (Cummings and Arnott, 2005) as extensive allochthonous salt bodies were emplaced on the Scotian Slope.

Hydrocarbon charge in the Scotian Basin mostly took place during the Cretaceous (Williamson 1995; OETR 2011). Karim et al. (2011, 2012) documented primary fluid inclusions in silica overgrowths and carbonate cements that only very rarely show fluorescence indicating the presence of hydrocarbons, and secondary fluid inclusions in trains in fractures that commonly contain hydrocarbons. The primary fluid inclusions in cements indicate a period of flow of hot basinal brines (<175 °C, <23 wt% NaCl) during the Aptian-Albian (middle Cretaceous). Other evidence for a mid-Cretaceous thermal event in the Scotian Basin is late Aptian volcanism in the Orpheus graben and enhanced

heat flow in terrestrial basins (Bowman et al., 2012). High heat flow combined with the abundant availability of salt in the Scotian Basin has resulted in unusual diagenetic minerals such as sphalerite, barite and hydrothermal zircon (Pe-Piper et al. 2015, 2017).

4.3. Previous works on titania minerals and hydrocarbons

Titania (TiO_2) has three polymorphs: rutile, anatase and brookite. The polymorphs all share the same chemistry, but each has a different and specific structural arrangement of atoms. Rutile and anatase have a tetragonal crystal structure, whereas brookite has an orthorhombic crystalline structure (Figs. 3a-c) (Regonini et al. 2013). Rutile has a tetragonal unit cell, with cell parameters a= b = 4.584 Å, and c = 2.953 Å where the titanium cations have coordination number of 6 and are surrounded by an octahedron of 6 oxygen. The oxygen anions have a coordination number of 3, resulting in a planar coordination (Fig. 3a). Anatase also has a tetragonal unit cell, but with cell parameters a = b = 3.7845 Å, c = 9.5143 Å. The titanium cations have a coordination number of 4 and are surrounded by 4 oxygen ions (Fig. 3b). Brookite has an orthorhombic crystal structure with unit cell parameters a = 5.4558 Å, b = 9.1819 Å and c = 5.1429 Å. The titanium cations have a coordination number of 6 and are surrounded by an octahedron of 6 oxygen, each octahedron shares three edges with adjoining octahedra forming an orthorhombic structure (Fig. 3c). At any set of physical conditions (e.g. temperature, pressure and pH) one structure is more stable than the other. The structure with the lowest energy, if formed under a condition in which it favours, will precipitate over the other polymorphs.

Laboratory study of nano-scale growth of authigenic titania show that the first polymorph to precipitate is anatase, but that as crystal size increases , this inverts first to brookite (>11 nm) and then to rutile (>35 nm) (Zhang and Banfield, 2014). However, both anatase and brookite occur as micron-scale crystallites in loose aggregates in black shales (Schulz et al. 2016). In natural systems, growth and stability of the two polymorphs is mainly controlled by local pH conditions (Zhang and Banfield, 2014). Rutile forms at very low pH (<3), whereas anatase forms at high pH (>5) and brookite forms at low pH (3–6) (Li et al. 2007; Schulz et al. 2016).

Titania phase transformation is also affected by temperature. Rutile mostly occurs in high grade metamorphic and some igneous rocks whereas anatase and brookite are considered to be the low temperature and low pressure titania polymorphs (Meinhold, 2010). In chemical syntheses, availability of complexing ions highly affects titania phase transformation. Non-complexing ions favour rutile formation, whereas sulphate (SO^{2-}_4) and fluorine (F) ions favour anatase, and increasing F^- prevents formation of brookite and prevents anatase to rutile transformation (Pottier, 2001; Yu et al. 2002). Chloride (Cl^-) ions are necessary for brookite formation and prevent brookite recrystallization to rutile (Pottier, 2001; Li et al. 2007). At a nano scale, Niobium (Nb) doping hinders anatase growth and facilitate anatase to rutile phase transformation (Arboil et al. 2002). Aluminium (Al) has no influence on titania phase composition (Lee et al. 2004). Other important variables include chemistry of ambient fluids including organic acids and redox conditions, particularly the valence state of Vanadium (V) (Li et al., 2010; Liu et al., 2019).

Sandstone diagenesis in the Scotian Basin involved a complex succession of mineral cements and the development of secondary porosity (Zhang et al. 2015). Sea-floor diagenesis in proximal settings is dominated by the effects of abundant iron, resulting in Fe-rich clays, siderite and phosphates, while in distal settings early calcite cements are more common (Okwese et al. 2012). Sea level lowstands promoted the flux of meteoric water resulting in local development of abundant kaolinite cement (Karim et al. 2010). At greater burial depths, first quartz overgrowths and then pore-filling Fe-calcite or ankerite are common (Karim et al., 2010). In some wells, chlorite rims on framework quartz grains inhibited quartz cementation and preserved porosity (Gould et al., 2010). At burial depths >2 km, K-feldspars are dissolved or replaced by diagenetic albite (Pe-Piper, 2012). In many wells, both quartz and carbonate cements are fractured, with pervasive development of secondary porosity. Secondary fluid inclusions related to this fracturing contain hydrocarbons (Karim et al. 2012). Such secondary porosity is filled with a wide range of late cements including illite, chlorite, kaolinite, siderite, barite and sphalerite (Pe-Piper et al. 2015). Hydrothermal zircons are also present as neoformed minerals partially filling porosity or as diagenetic outgrowths on detrital zircon grains (Pe-Piper et al. 2017).

Diagenesis of titania minerals in the Scotian Basin was previously studied by Pe-Piper et al. (2011). The authors established two occurrences of authigenic titania, during early diagenesis (eogenesis) and late diagenesis (mesogenesis). Eodiagenetic titania replaces non-compacted detrital fragments of plant material (phytodetritus) and as concentric layers filling intergranular pore spaces bounded by quartz grains lacking

overgrowths and is associated with eodiagenetic kaolinite. Mesodiagenetic titania has a lower P content and is associated with secondary porosity or occurs as pseudomorphs of flattened phytodetritus. Pe-Piper et al. (2011) proposed that during eodiagenesis, Ti mobility was facilitated by the presence of meteoric waters that contain humic acids at lowstand boundaries, whereas Ti mobility during mesodiagenesis was due to the release of organic acids during the early stages of hydrocarbon migration.

Titanium is commonly hosted in Ti-rich detrital minerals. In many basins, Ti is supplied principally from titanomagnetite, ilmenite, biotite and amphibole (Morad and AlDahan, 1986; Liu et al., 2019). The shales of the Scotian Basin have Ti abundance (1 wt% Ti), double that of global average shales (Pe-Piper et al., 2008), suggesting unusually abundant supply of Ti by rivers. This supply was principally as detrital grains of ilmenite and their alteration products (Pe-Piper et al. 2005). This is also supported by the observation of Ledger (2014) that detrital titania minerals in the Scotian Basin often show signs of dissolution or partial dissolution. Detrital titania minerals are thus present in Scotian Basin sandstones with abundance of up to 3% by volume (Pe-Piper et al. 2011) and many show signs of partial dissolution or replacement (Ledger, 2014).

4.4. Materials and Methods

4.4.1 Sampling strategy

Diagenetic titania minerals were studied from polished thin sections made from sandstones from conventional cores provided by the Canada-Nova Scotia Offshore Petroleum Board (CNSOPB) Geoscience Research Centre. Overall, 16 wells and 65

samples were selected to cover a range of parameters such as: hydrocarbon presence, temperature and salinity interpreted from fluid inclusions, burial depth, and stratigraphic level (Fig. 2). The samples are from the Upper Jurassic to Middle Cretaceous sandstones with burial depths of 2–6 km in the Central to Eastern part of the Scotian Basin, with a focus on four known oil and/or gas producing fields: the Venture, Thebaud, Glenelg and Cohasset-Panuke fields. The first three fields have overpressured sandstone reservoirs in roll-over anticlines bounded by listric growth faults; traps in the Cohasset-Panuke field are in a subtle fold about a basement element. Targeted sandstones in other wells were in folds related to salt (e.g. Louisbourg J-47) or basement highs (Peskowesk A-99, Kegeshook G-67) or stratigraphic traps (Onondaga O-95, South Desbarres O-76) or in thrust-related fold on the upper slope (Newburn H-23). Descriptions of sandstone lithofacies follow Gould et al. (2012). The polished thin sections were studied under petrographic microscope to locate titania minerals. The titania grains were then studied using various techniques.

4.4.2. Analytical techniques

4.4.2.1. Scanning electron microscope (SEM)

The scanning electron microscope (SEM) was mainly used to acquire backscattered electron images to define textural and morphological characterization of diagenetic titania minerals (Appendix 1-9). The images were collected using a TESCAN MIRA 3 LMU Variable Pressure Schottky Field Emission SEM equipped with an INCA X-max 80 mm^2 silicon drift detector (SDD), Energy Dispersive Spectrometer (EDS) and

Backscattered Electron (BSE) detector. EDS was used for quick mineral identification. The EDS system has a detection limit of < 0.1%. A pure cobalt plate was used as a standard to calibrate the beam for analysis. The beam has an average diameter of approximately <10 nm and has an X-ray production volume of ~10 μm. The SEM has a maximum resolution of 1.2 nm at 30kV. All analyses were acquired using a power of 20 kV.

4.4.2.2. Laser Raman spectrometry

Raman spectra were collected to distinguish the titania minerals rutile, anatase and brookite (Appendix 1-5). The analysis was performed at the Regional Analytical Centre at Saint Mary's University using a Horiba Jobin-Yvon LabRam HR confocal instrument. The instrument uses a 100 mW 532 nm Nd-YAG diode laser from Toptica Phonotics and a Synapse charge-coupled device form Horiba Jobin-Yvon. It uses a maximum of 100x Olympus MPlanN objective for image capture and analysis.

Analyses were acquired using a 25 μm confocal hole diameter, and 600 grooves/mm grating was used for all analyses, yielding a spectral resolution of approximately ±2 cm. Spectra were collected using an accumulation of three twelve-second acquisitions with a laser spot size of approximately 1 μm at 50% laser power. The spectra were collected in two spectral windows 200–4000 cm^{-1} and 200–2600 cm^{-1}. Analysed samples had carbon coating removed using methanol to increase the intensity of the peaks and to ensure more accurate results. Raman spectra for rutile, anatase and brookite were referenced from Meinhold (2010), Triebold et al (2011) and the RRUFFF database.

4.4.2.3. Electron microprobe (EMP) analysis

Major and selected minor element compositions of diagenetic titania minerals (Appendix 10-11) were obtained using a JEOL-8200 electron microprobe (EMP) at the Regional Electron Microprobe Centre at Dalhousie University, in Halifax. The microprobe is equipped with a Noran 133 eV dispersive spectrometer and five wavelength spectrometers. The equipment was operated at 15 kV and 20 nA with a beam diameter of 2 µm. A complete set of all the analyses and standards is available in Appendix 10 or 11.

4.4.2.4 Information on geological setting of samples

General information on wells is from the Basin database (https://basin.gdr.nrcan.gc.ca/wells/index_e.php). Information on free water levels in producing fields is based on SOEP (Sable Offshore Energy Project) Development Plan Application and CNSOPB (Canada – Nova Scotia Offshore Petroleum Board) 2000 Technical Summaries of Scotian Shelf Significant and Commercial Discoveries. Comparison with fluid inclusion data is based on data in Karim et al. (2011, 2012) and Hanley (2011). Sequence stratigraphy and lithofacies (Table 1, fig. 2) are interpreted from Cummings and Arnott (2005), Cummings et al. (2006), Karim et al. (2010) and Gould et al. (2012).

4.5. Results

4.5.1. Raman spectroscopy

Rutile was identified using Raman bands or peak positions at 240, 450 and 615 cm^{-1} (Fig. 3d), whereas anatase was identified using peak positions at 143, 400, 516 and 642 cm^{-1} (Fig. 3e). Brookite produced a range of Raman bands and was identified at peak positions of 128, 155, 215, 247, 250, 289, 323, 368, 453, 549 and 638 cm^{-1} (Fig. 3f). Identifications were confirmed by comparison with titania reference spectra from Triebold et al (2011). More than 96% of the analyses of titania minerals in the Scotian Basin occur as pure phases, but occurrences of mixed spectra between the three titania polymorphs with varying relative intensities have also been observed (Fig. 3g-i). Mixed analyses between anatase and rutile are most common (Fig. 3g-h) followed by mixed analyses of brookite and rutile (Fig. 3i). A mixture of anatase and brookite was not observed. With a 2 μm resolution of the analysed spot, acquired mixed spectra may be derived from microscopic phase boundaries between overlapping titania grains or from a sub-μm phase mixture.

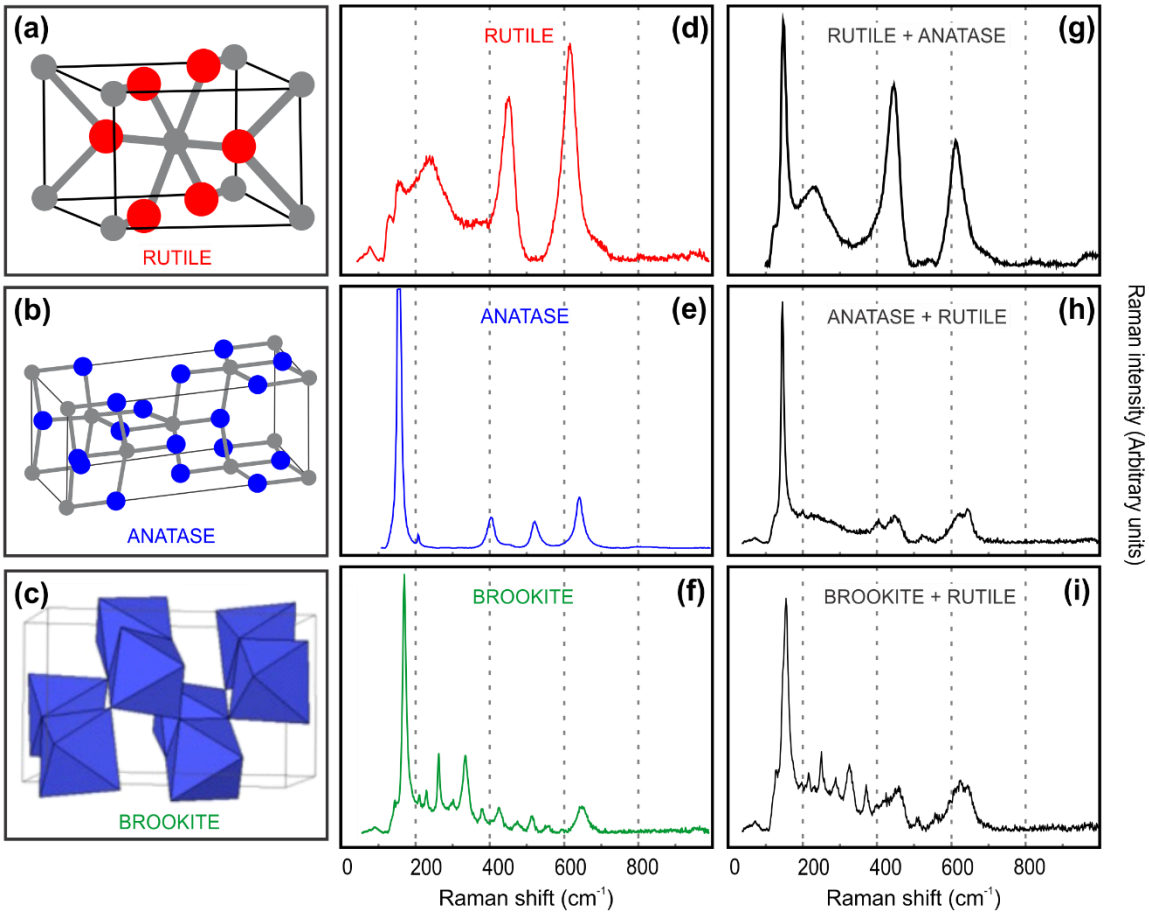

Figure 3. Crystal structure (Regonini et al. 2013) and examples for Raman spectra of titania minerals in the Scotian Basin. **(a-c)** Crsytal structure of rutile, anatase and brookite. **(d-f)** Pure spectra of rutile, anatase and brookite. **(g-h)** Mixed spectra between rutile and anatase. **(i)** Mixed spectra between brookite and rutile.

4.5.2. Optical properties

Titania minerals in the Scotian Basin sandstones are either of detrital or diagenetic in origin. Under transmitted light in a petrographic microscope, detrital titania grains are mostly opaque (Fig. 4a), with rounded edges. Diagenetic titania minerals in the same rock show textures interpreted as either replacive or neoformed. In general, replacive titania grains have similar properties to detrital titania grains, which may be due to the residual detrital titania (Fig. 4b). Replacive titania are commonly opaque with black to dark red

color and often appear to have a dusty black cloud. Neoformed titania minerals are less opaque to completely translucent. They have lighter colour, light brown to yellowish brown to pale yellow. They occur either as granular aggregates (Fig. 4c) or a well-defined euhedral crystals with straight black edges and sharp corners (Fig. 4d).

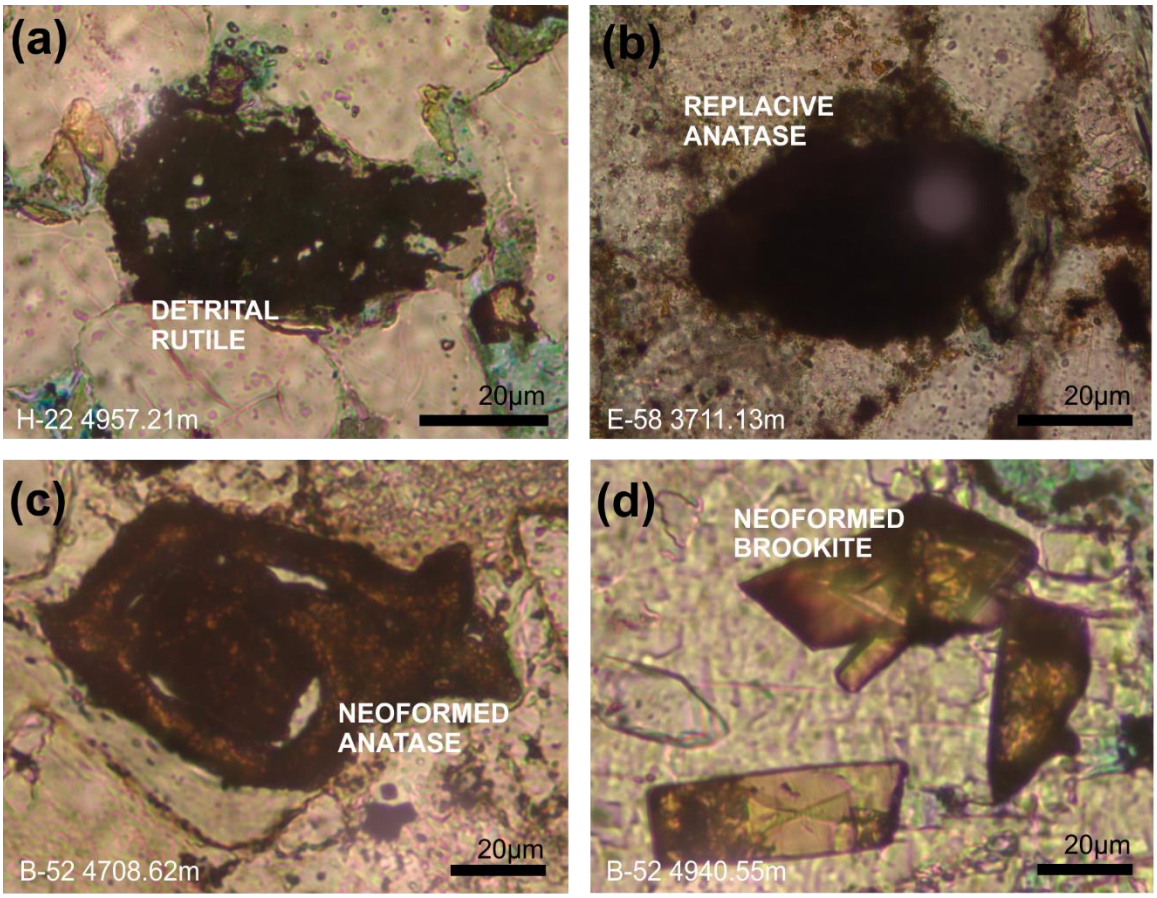

Figure 4. Titania minerals under transmitted light microscope. **(a)** Opaque detrital rutile. **(b)** Dark to opaque replacive anatase. **(c)** Aggregates of neoformed anatase. **(d)** Euhedral neoformed brookite crystals.

Diagenetic rutile often shows yellow, light brown to red colours. Diagenetic anatase is common as aggregates and shows brown with hints of yellow to reddish brown colour (Fig. 4c). Diagenetic brookite is mostly brownish-yellow to light yellow under

transmitted light (Fig. 4d). Diagenetic rutile, anatase and brookite cannot be distinguished in all cases using optical microscopy. Doubts in identification arise due to the similarity in morphology of diagenetic rutile and anatase, and similar colour of anatase and brookite. Both diagenetic anatase and brookite may have straight edges and may have similar colours, and diagenetic rutile often occurs in aggregates similar to anatase.

4.5.3. Morphology (based on Back-scattered electron images)

Back-scattered electron (BSE) images of diagenetic titania minerals in the Scotian Basin sandstones typically exhibit three main types of morphology: (1) euhedral to subhedral clean crystal grains with sharp corners and straight edges (Fig. 5a); (2) euhedral to subhedral grains with visible dissolution voids or clay inclusions (Fig. 5b); (3) anhedral, sponge-like crystal aggregates (Fig. 5c). Type 1 is the dominant morphology of all of the studied diagenetic titania minerals, especially neoformed titania minerals. Replacive titania typically displays Type 3 morphology. Type 2 morphology is most common in titania minerals of the Glenelg and Thebaud fields. Most rutile exhibits Type 2 or 3 morphology, anatase is most commonly seen with Type 1 or Type 3 morphology (Figs 5a and 5c), whereas brookite principally displays Type 1 morphology (Figs. 5a, brookite not in figure, 5e).

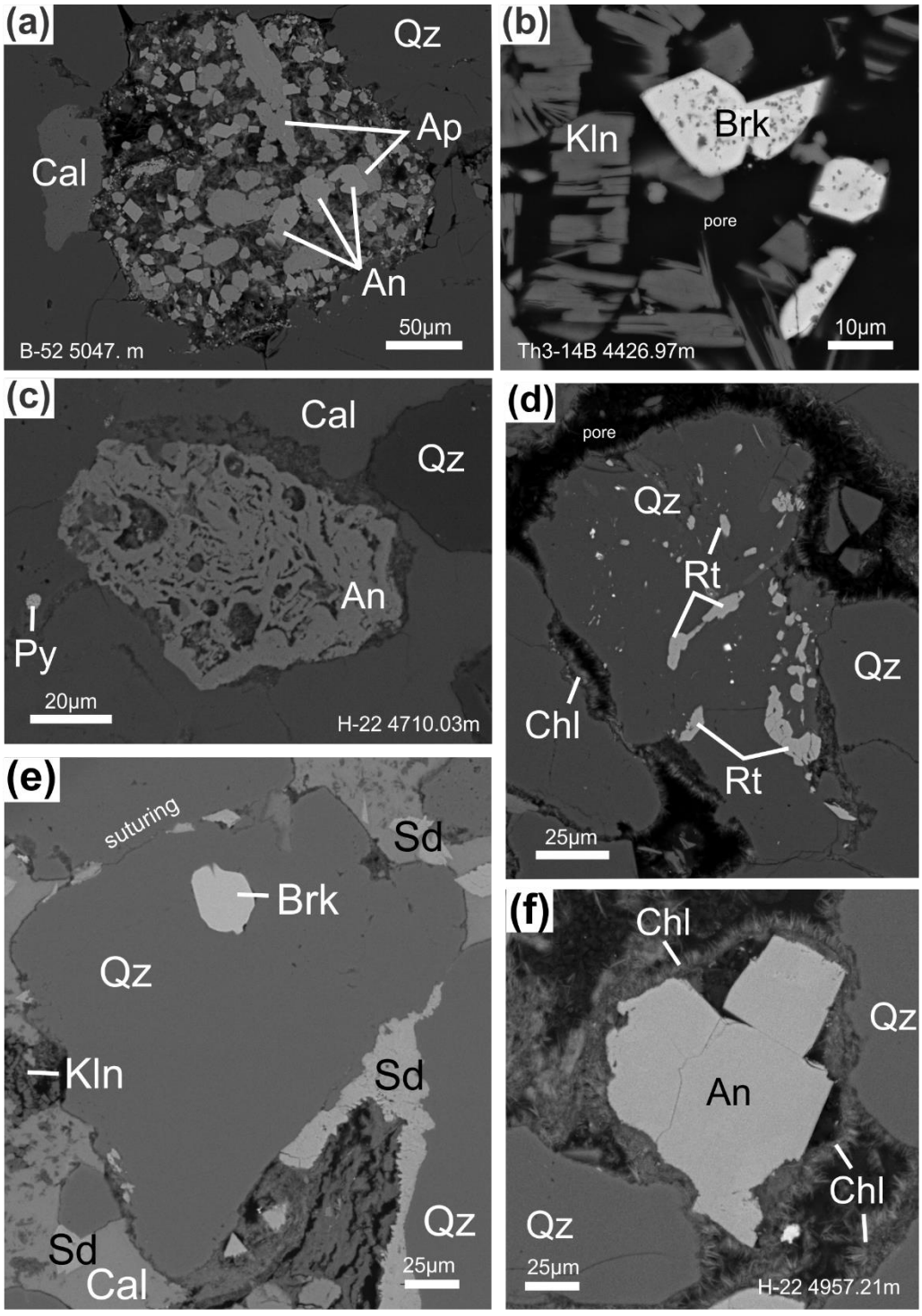

Figure 5. Representative backscattered electron images of morphology of diagenetic titania minerals. **(a)** Euhedral to subhedral crystals of anatase (An) occurring in pore with diagenetic apatite (Ap). **(b)** Euhedral crystals of brookite (Brk) with clay inclusions in pore with diagenetic kaolinite (Kln). **(c)** Sponge-like anatase fills pore in calcite cement. **(d)** Diagenetic rutile fills fractures in quartz. **(e)** Brookite fills cavity in quartz crystal. **(f)** Diagenetic anatase rimmed by chlorite rims.

4.5.4. Textural relationships (based on Back-scattered electron images)

4.5.4.1. Textural relationships in general

Back-scattered electron images of diagenetic titania polymorphs show the minerals occur either as a replacement or a neoformed mineral. The term replacement is used to indicate the precipitation of a new mineral within a pre-existing mineral that may or may not incorporate some of the chemical components and/or crystal structure of the parent mineral. All replacements are introduced via a dissolution/reprecipitation mechanism (Altree-Williams et al., 2015). In contrast, the term neoformed is used to indicate direct precipitation in porosity from the solution.

Rutile is mostly detrital, most commonly occurring as framework grains, some showing textures suggesting alteration of ilmenite (Fig. 6a). Diagenetic rutile generally occurs as neoformed irregular rims around a quartz crystal boundary (Fig. 6b). Diagenetic anatase occurs both as neoformed and replacive. Anatase replaces mostly detrital rutile and pseudomorphs uncompacted phytodetritus in samples with quartz framework grains lacking overgrowths (Fig. 6c). However, anatase largely occurs as euhedral to subhedral neoformed titania in pores and fractures along sutured quartz boundaries (Fig. 6d). Similar to anatase, diagenetic brookite occurs as either replacive or neoformed. Replacive brookite only occurs together with anatase, replacing detrital rutile. Neoformed brookite is predominantly cement, mostly occurring either as a single isolated euhedral crystal (Fig. 6e) or as a cluster of euhedral-subhedral crystals with clay minerals against euhedral quartz overgrowths in pores (Fig. 6f, yellow arrows indicate quartz overgrowth), fractures, and along intergranular boundaries of quartz grains.

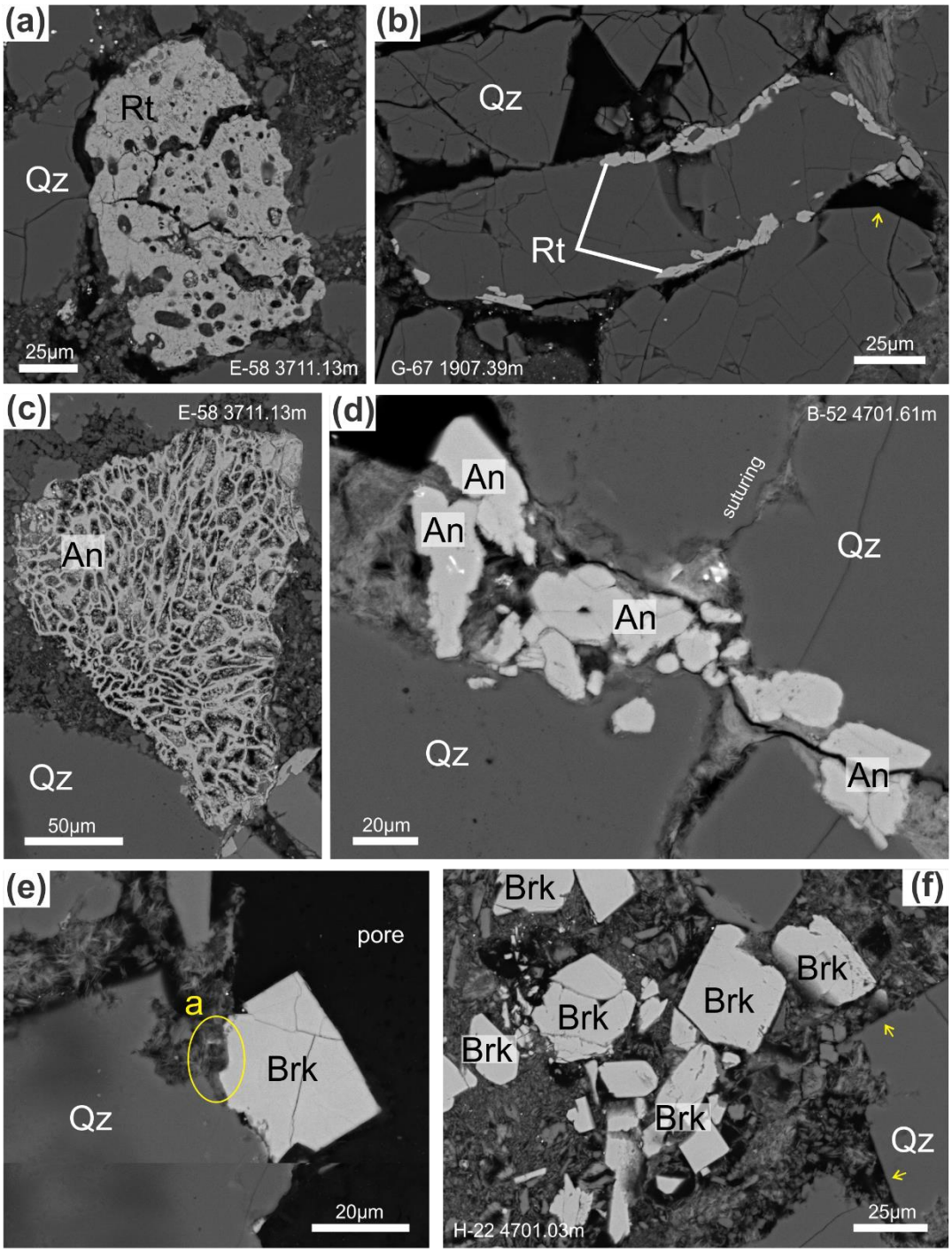

Figure 6. Representative backscattered electron images of main occurrences of diagenetic titania minerals. **(a)** Ilmenite grain pedogenically altered to rutile (Rt). **(b)** Diagenetic rutile rimming quartz overgrowth. **(c)** Anatase (An) replacing uncompacted phytodetritus with quartz (Qz) framework grains lacking overgrowths. **(d)** Cluster of euhedral anatase precipitating along fracture of sutured quartz. **(e)** Isolated crystal of brookite in pore semi-attached to a framework quartz grain **(f)** Cluster of clean brookite (Brk) crystals with straight edges in pore. Yellow arrows indicate quartz overgrowths.

4.5.4.2. Textural relationship in oil and gas-producing fields

Diagenetic anatase in the Panuke-Cohasset field fills pores of dissolved framework grains typically cemented by early calcite (Fig. 7a) or fills pores within calcite cement (Fig. 7d, position a). Diagenetic brookite precipitates along intergranular boundaries of sutured quartz, overprinting overgrowths (Fig. 7b). Relative timing of late anatase and brookite is shown in sample Cohasset A-52 2230.38m, where clean euhedral brookite with a straight edge partly fills a pore of dissolved calcite cement already partly filled by euhedral anatase, which is engulfed by the brookite (Fig. 7a, position a).

In the Glenelg field, anatase commonly pseudomorphs phytodetritus (Fig. 6c) or detrital rutile. Euhedral grains of diagenetic brookite precipitate in pores and engulf calcite and kaolinite (Fig. 7c). Similar to the Glenelg field, small aggregates of anatase in the Thebaud field pseudomorph phytodetritus which seems to be engulfed by quartz overgrowths (Fig. 7f, yellow arrows indicate quartz overgrowth). A thin crystal lath of brookite in Thebaud field forms in intergranular spaces of framework quartz and appears to overprint or replace chlorite that rims quartz crystal boundaries (Fig. 7e, position a). Diagenetic anatase in a deep limestone in the Venture field typically fills pores starting from the rim in partly dissolved calcite with occasional residual quartz in the core (Fig. 7h). In sample H-22 4957.21m, euhedral crystals of late anatase fill a dissolution cavity rimmed by chlorite, postdating both phases of chlorite rims (Fig. 5f). Diagenetic brookite forms euhedral to subhedral crystals in pores of calcite cement, but also fills pore spaces and fractures between quartz grains, replacing chlorite rims and quartz overgrowths (Fig. 7g, position a).

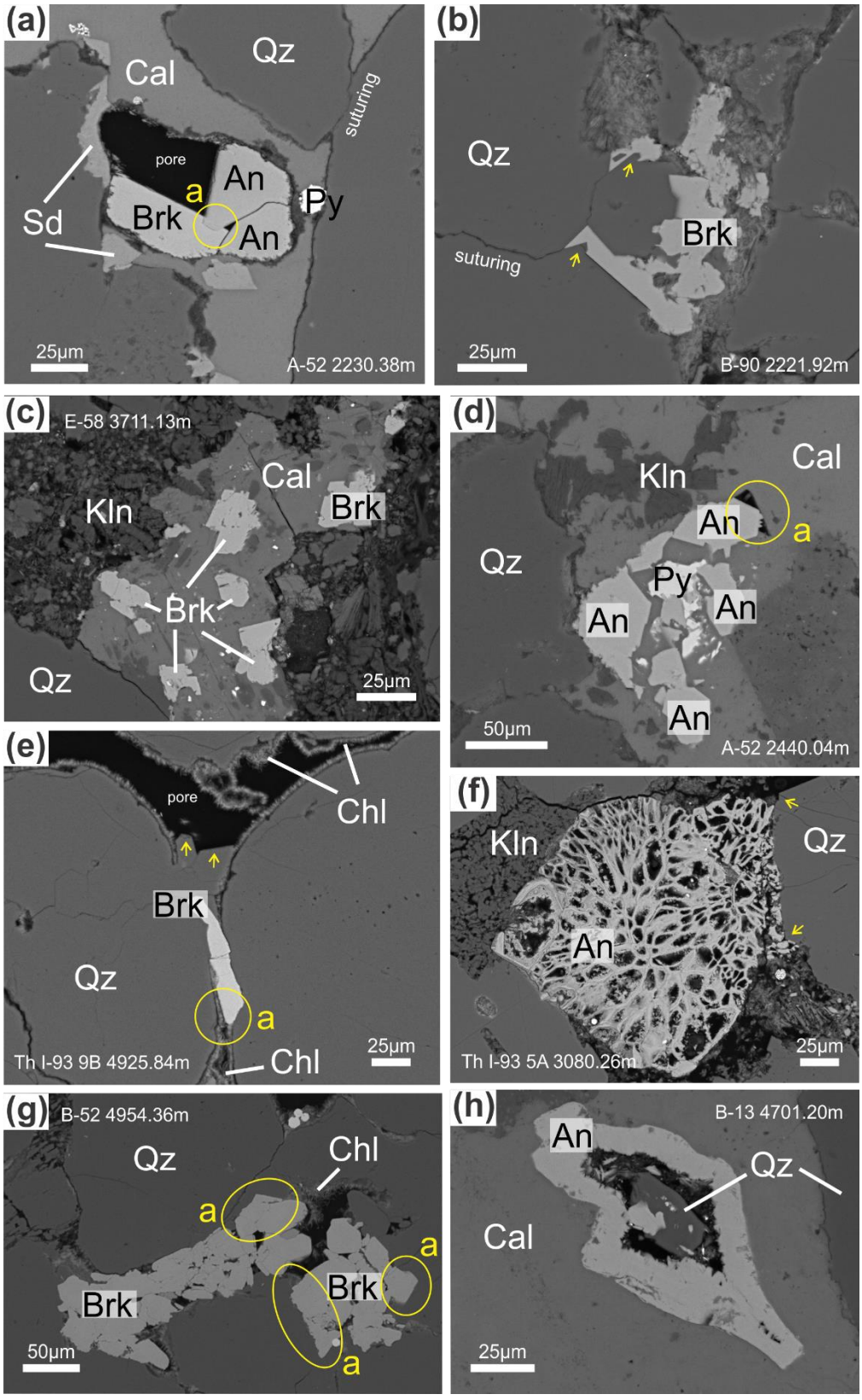
(a)
Cal
Qz
suturing
pore
An
a
Py
Sd
Brk
An
25μm
A-52 2230.38m
(b)
Qz
Brk
suturing
25μm
B-90 2221.92m
(c)
E-58 3711.13m
Cal
Kln
Brk
Brk
Qz
25μm
(d)
Kln
Cal
An
a
Qz
Py
An
An
An
50μm
A-52 2440.04m
(e)
pore
Chl
Brk
Qz
a
Th I-93 9B 4925.84m
Chl
25μm
(f)
Kln
Qz
An
Th I-93 5A 3080.26m
25μm
(g)
B-52 4954.36m
Qz
Chl
a
a
Brk
Brk
50μm
a
(h)
B-13 4701.20m
An
Qz
Cal
25μm

Figure 7. Representative backscattered electron images of occurrences of diagenetic titania from four oil- and/or gas-producing fields (Panuke-Cohasset, Glenelg, Thebaud and Venture fields). **(a)** Brookite and anatase fills a framework pore. **(b)** Brookite occurring along quartz grain boundaries, engulfing overgrowths. **(c)** A cluster of brookite in partly dissolved calcite cement. **(d)** Cluster of clean anatase crystals in calcite cement with pyrite. **(e)** A single brookite in intergranular quartz boundary overprinting chlorite rims. **(f)** Pseudomorphic anatase replacing phytodetritus material. **(g)** Cluster of euhedral brookite crystals filling pore along intergranular quartz boundaries. **(h)** Anatase rims pore with residual quartz in the center in calcite cement. Yellow arrows indicate quartz overgrowths.

4.5.4.2. Textural relationships in other wells

Diagenetic anatase and brookite in South Desbarres O-76 form as blocky crystals and fill pores surrounded by framework quartz without overgrowths (Fig. 8a, only brookite). Replacive anatase in Onondaga O-95 replaces partially dissolved detrital rutile or fills pore of residual framework grain (Fig. 8b). Brookite in Newburn H-23, either occurs as a single euhedral crystal, enclosed by or attached to quartz, or as cluster of crystals in a pore, rimming quartz (Fig. 8c), whereas sponge-like anatase occurs along a quartz grain boundary, preventing quartz overgrowths and thus likely eogenetic (Fig. 8d, yellow arrows indicate quartz overgrowths). In Kegeshook G-67, diagenetic anatase partially replaces or partially fills pores with relics of framework grains (Fig. 8e). Brookite occurs as euhedral crystals in pores with siderite or engulfs framework detrital quartz grains. Diagenetic titania in Peskowesk A-99 is entirely brookite and usually occurs as blocky or lath-like crystals. It mostly occurs either as a single crystal in a pore or as a cluster of crystals in a pore cross-cutting kaolinite that has replaced earlier framework minerals (Fig. 8f).

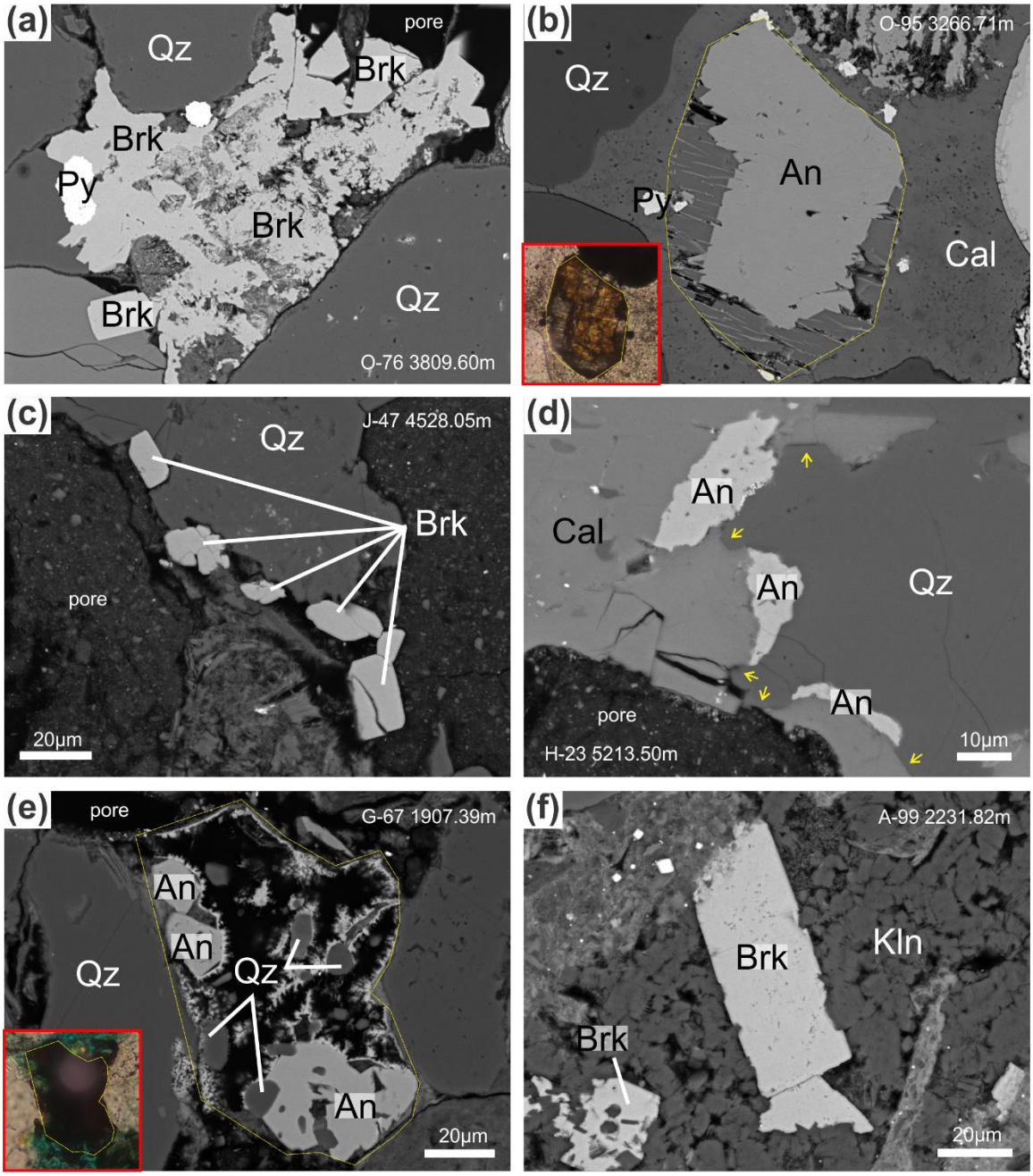

Figure 8. Representative backscattered electron images of diagenetic titania minerals from other wells (South Desbarres O-76, Onondaga O-95, Louisburg J-47, Newburn H-23, Kegeshook G-67, Peskowesk A-99). **(a)** Brookite (Brk) precipitating clean crystals with straight edges outwards. **(b)** Diagenetic anatase (An) and calcite (Cal) replaced a framework grain. **(c)** A string of euhedral brookite crystals occurring along a fracture. **(d)** Sponge-like anatase in between calcite and quartz (Qz) crystal boundary engulfing quartz overgrowths. **(e)** Anatase partially replacing a framework grain with quartz**. (f)** Brookite crystals in pore engulfed by booklets of kaolinite (Kln). Yellow arrows indicate quartz overgrowths.

4.5.5. Abundance and distribution

Overall, anatase and brookite are the most common diagenetic titania polymorphs in the Scotian Basin (Table 1). Diagenetic rutile is rare. Anatase as a replacement of a TiO_2 mineral is most common in samples with high amounts of detrital rutile. The four studied oil- and or gas-producing fields in the Scotian Basin (Panuke-Cohasset field, Glenelg field, Venture field and Thebaud field) show all phases of titania minerals, however diagenetic anatase and brookite dominate over diagenetic rutile.

Diagenetic titania minerals from reservoir sandstones of the Thebaud and Venture fields show that anatase predominantly occurs below estimated free water levels whereas brookite mainly occurs in the hydrocarbon reservoir interval (Fig. 9). In the Glenelg field, brookite is found in both the water and gas interval whereas lesser anatase is present only below the estimated free water level (with the exception of one grain above). Titania minerals in the Cohasset field show similar pattern to both the Thebaud and Venture fields. Anatase occurs below the free water level whereas brookite is concentrated above. In the Panuke field, no distinctive separation between anatase and brookite were observed.

Wells with minor hydrocarbon or no hydrocarbons also have anatase and brookite as the dominant phases of diagenetic titania. Onondaga O-95 and Louisburg J-47 wells both have minor amounts of hydrocarbons, whereas South Desbarres O-76, Newburn H-23, Kegeshook G-67 and Peskowesk A-99 lack hydrocarbons. Anatase appears to be more abundant in wells with minor hydrocarbons while brookite is dominant in wells

lacking hydrocarbons. Collectively, all these wells have water dominant over hydrocarbons and are referred to as “wet wells”.

Other variations in abundance of particular polymorphs can be tentatively linked to other environmental factors summarized in Figure 2. There is a general tendency for the proportion of brookite to increase with depth (Table 1, Fig. 9), with the exception of the Venture field where anatase is particularly abundant (Table 1). The Venture field is unique among analysed fluid inclusion samples in having secondary carbonic (CO_2) inclusions (Karim, 2012). The Glenelg field is unusual in high proportion of brookite below the free water level. This might indicate that the reservoir had leaked and the hydrocarbon column was originally thicker, but diagenetic sphalerite is particularly abundant in the pores and cement in Glenelg field indicating flow of hot Cl^--rich fluids. Sphalerite is also relatively common in Louisburg and Peskowesk. However, anatase is common in Louisburg while brookite is common in Peskowesk (Table 1).

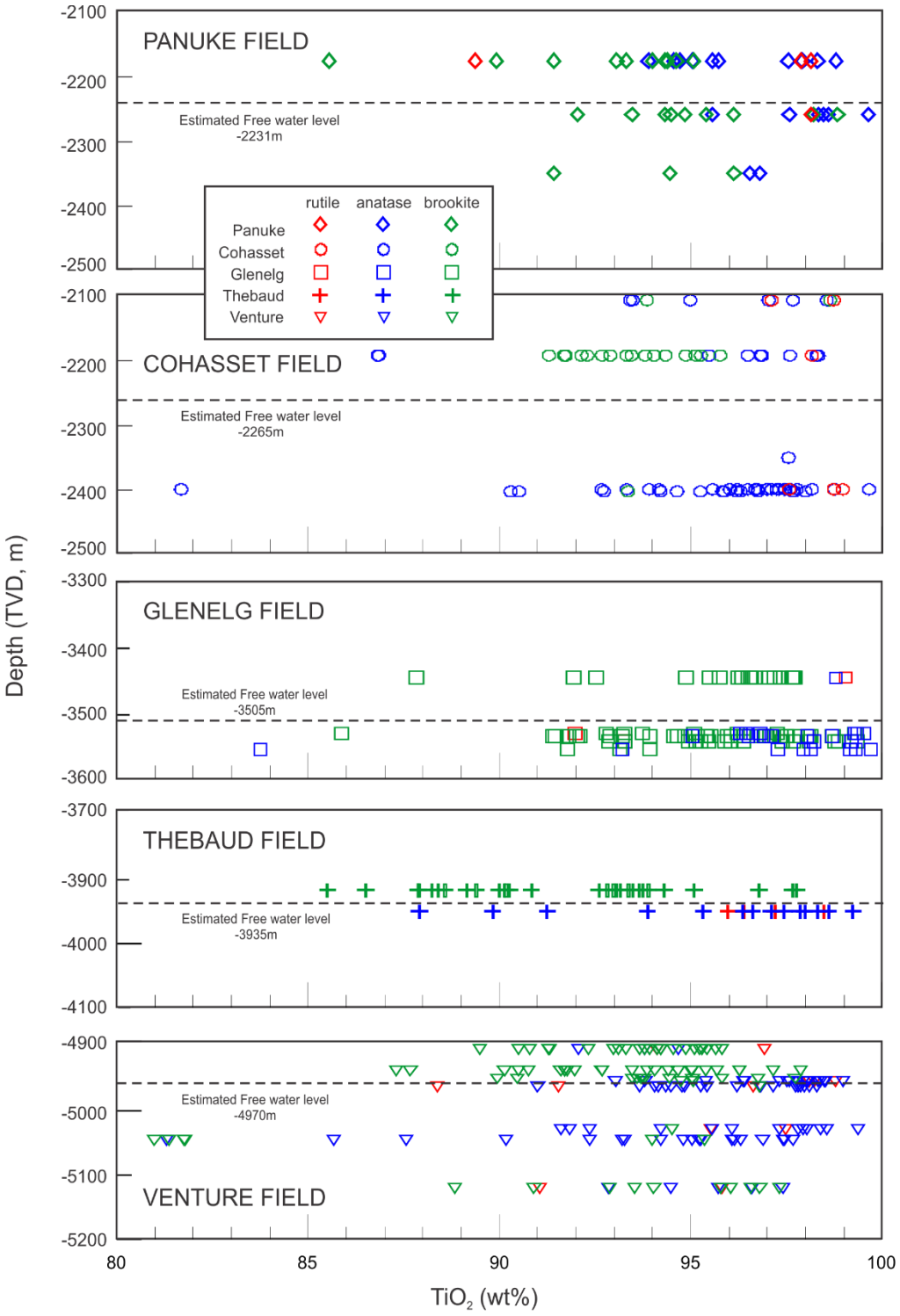

Figure 9. Distribution of all diagenetic titania minerals, both replacive and neoformed, in Panuke-Cohasset, Glenelg, Thebaud and Venture field in relation to each field's free water level.

4.5.6. Chemical composition

Diagenetic titania minerals from the Scotian Basin have relatively low TiO_2 concentrations. On average, diagenetic brookite has the lowest TiO_2 (mean 94.1 wt%) contents compared to both diagenetic anatase (~96.8 wt%) and diagenetic rutile (~96.1 wt%) (Fig. 10). In addition, concentrations of TiO_2 varies between the four studied oil and/or gas fields. Diagenetic anatase and brookite from Thebaud and Venture fields on average have lesser TiO_2 content (<94 wt%) compared to anatase and brookite from Panuke-Cohasset and Glenelg (>94 wt%). Furthermore, diagenetic anatase and brookite from Panuke-Cohasset and Glenelg have comparable TiO_2 content with analysed diagenetic anatase and brookite from wells lacking hydrocarbon, namely Peskowesk A-99, Kegeshook G-67 and Newburn H-23 wells (Fig. 10).

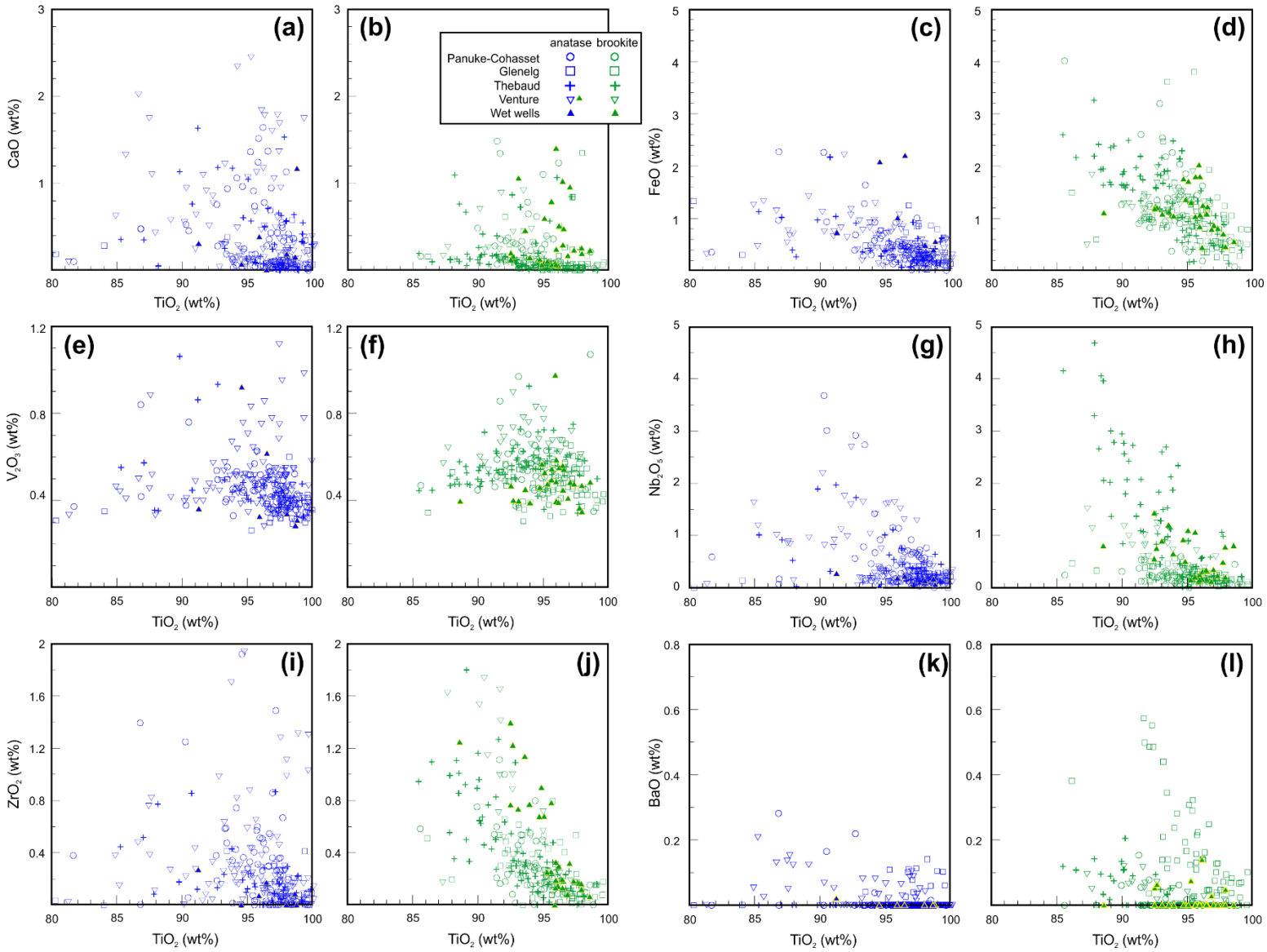
(a)
(b)
(c)
(d)
(e)
(f)
(g)
(h)
(i)
(j)
(k)
(l)
anatase brookite
Panuke-Cohasset
Glenelg
Thebaud
Venture
Wet wells
CaO (wt%)
FeO (wt%)
V2O3 (wt%)
Nb2O5 (wt%)
ZrO2 (wt%)
BaO (wt%)
TiO2 (wt%)

Figure 10. Binary plots showing geochemical compositional data for diagenetic brookite and anatase from the Scotian Basin.

In addition to the variations of TiO_2 concentrations, relatively high amounts of trace metal impurities are present in diagenetic anatase and brookite (Figs. 10, 11). The impurities differ between polymorphs and between oil-/gas-producing fields. In all four fields, brookite has elevated amounts of FeO (>0.6 wt%) and V_2O_3 (>0.55 wt%). However, in the Venture field, V_2O_3 is higher in anatase than brookite (Figs. 10e-f). Brookite from Thebaud field has high contents of Nb_2O_5 (Fig. 10d) while brookite from Glenelg field has elevated amounts of BaO (Fig. 10f). Brookite from wet wells also demonstrated higher amounts of Al_2O_3 when compared to anatase from the same wet wells (Figs. 11a-b). Both anatase and brookite have high SiO_2 (~0.57 wt%) and CaO (~0.3 wt%) contents, suggesting contaminations from quartz and residual calcite cement. Titania grains tend to be porous with inclusions and in addition, quartz and calcite cement can fill interstices within titania aggregates (Fig. 6a-f).

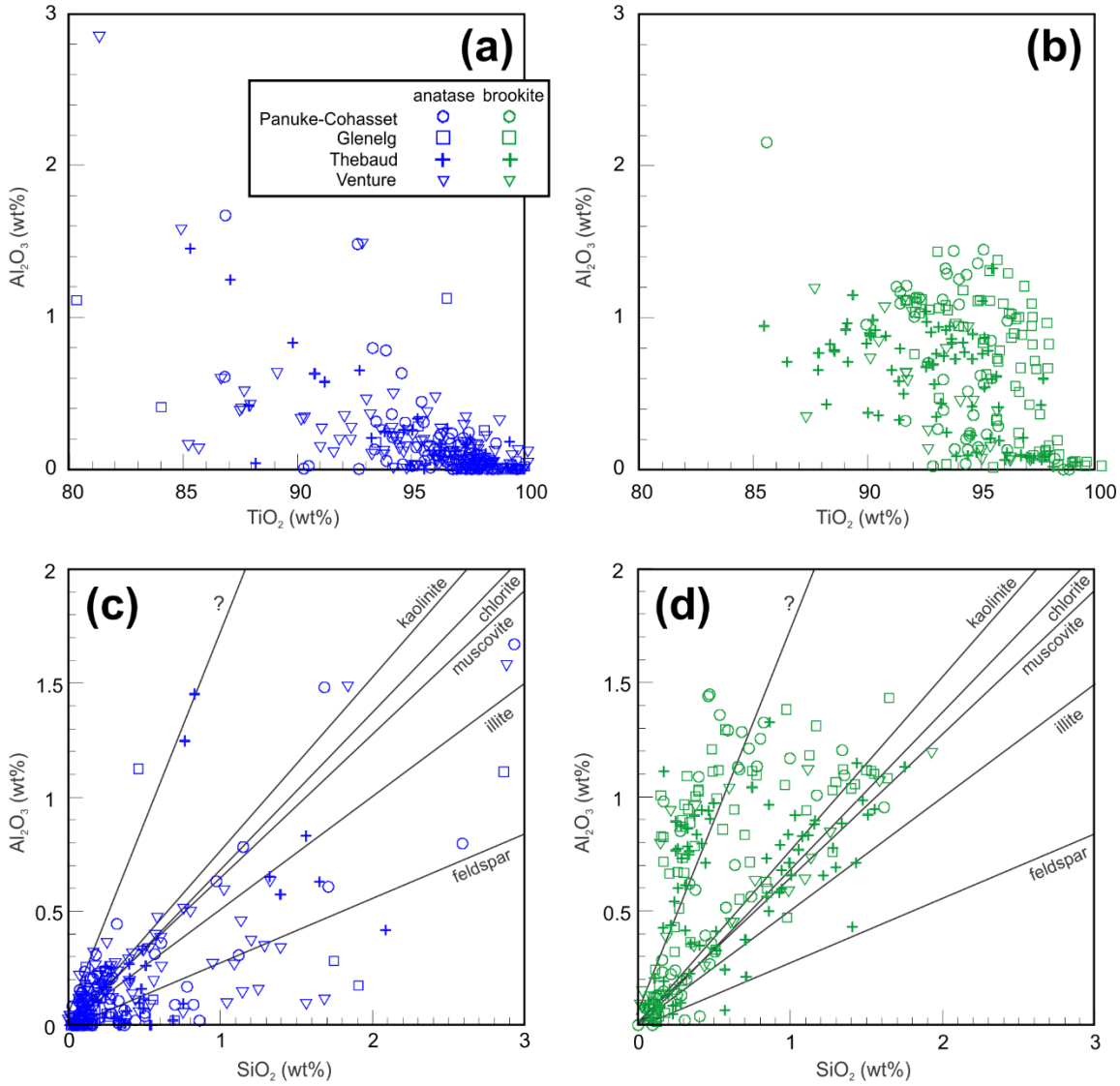

Figure 11. Binary plots of TiO_2 vs Al_2O_3 (a-b) and SiO_2 and Al_2O_3 (c-d) for titania minerals using EMP data.

Abundance of phosphorus within diagenetic titania has been previously used to separate early and late diagenetic titania (Pe-Piper et al, 2011). However, virtually all analyses from this study plot in the late diagenetic field with $P_2O_5 < 0.1$ wt%; only two

analyses of late anatase and one of late brookite fall within the early diagenetic field (Fig. 12).

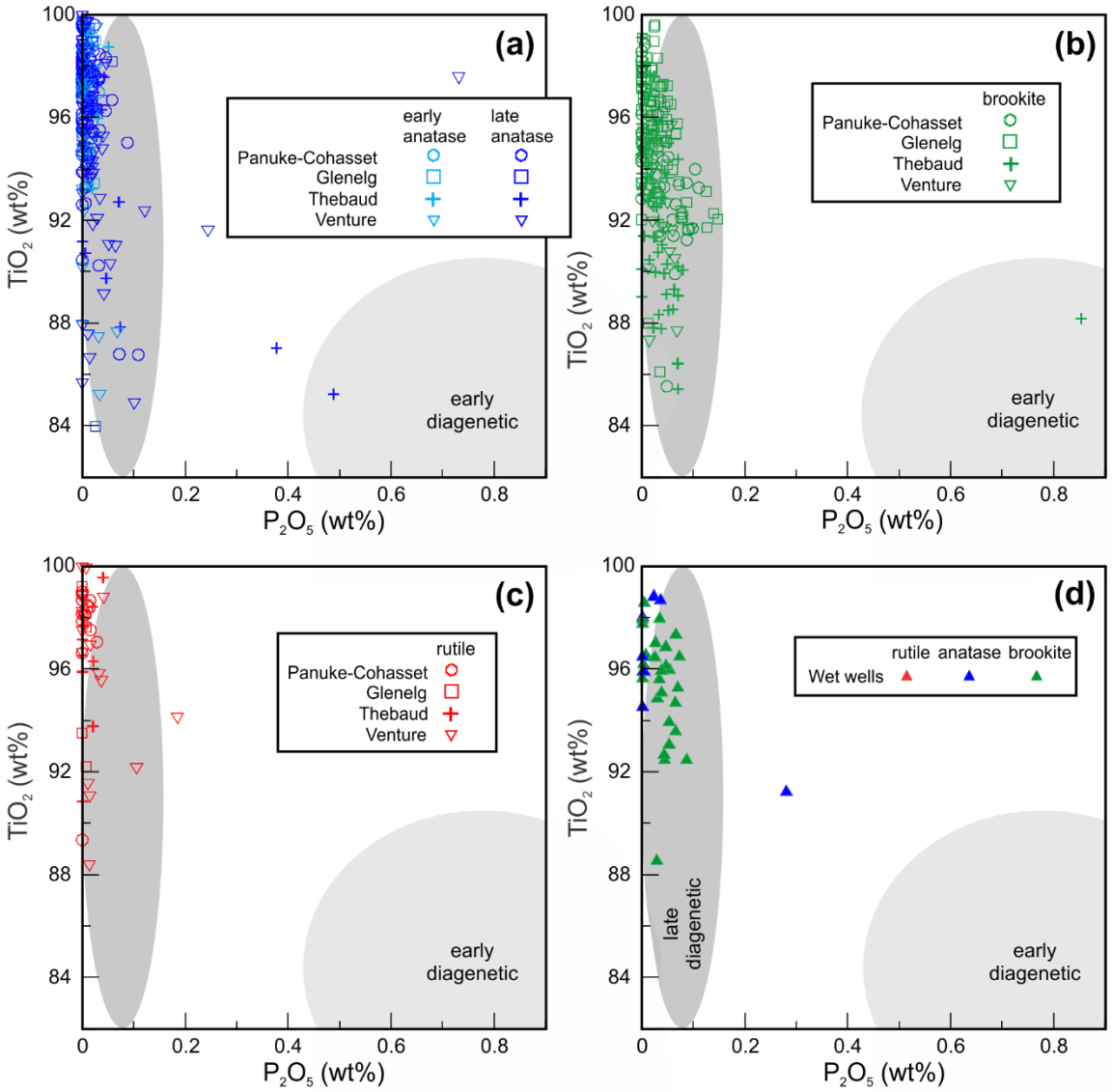

Figure 12. Binary plots of TiO_2 vs P_2O_5 for titania minerals using EMP data. **(a)** Diagenetic anatase from oil- and/or gas-producing fields. **(b)** Diagenetic brookite from oil- and/or gas-producing fields. **(c)** Diagenetic rutile from oil- and/or gas-producing fields. **(d)** TiO_2 vs P_2O_5 plot for titania minerals from hydrocarbon-lacking wells. Gray fields show the two occurrences of titania precipitation (Pe-Piper et al. 2011).

Chlorine (Cl) and fluorine (F) content within diagenetic titania minerals shows no variance between anatase and brookite. However, diagenetic anatase and brookite from oil-/gas-producing fields show higher Cl content (0-0.02 wt% Cl) compared to anatase and brookite from the wet wells Peskowesk A-99, Kegeshook G-67 and Newburn H-23 (<0.01 wt% Cl) (Fig. 13a). In addition, diagenetic titania minerals appear to have more F (up to 0.05 wt%) than Cl incorporated in their crystal structure (Figs. 13b).

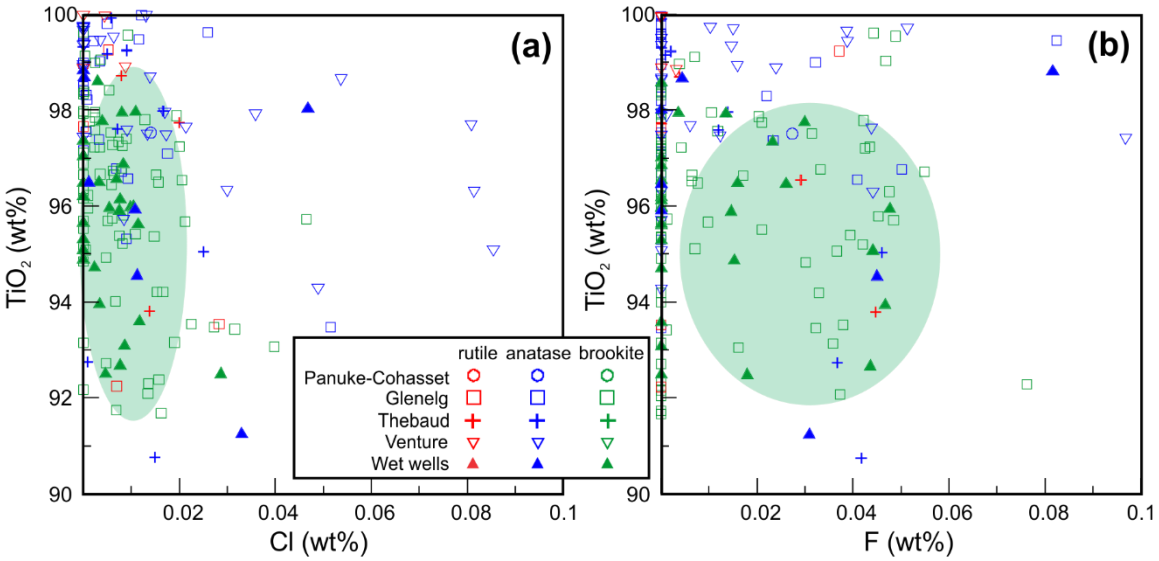

Figure 13. Binary plots of TiO_2 vs halogens (Cl and F) for diagenetic titania minerals using EMP data.

4.6. Discussion

4.6.1. Paragenetic sequence

Textural relationships of the titania polymorphs with other diagenetic minerals suggest at least two stages of titania precipitation (Fig. 14). Diagenetic titania minerals precipitated during early diagenesis (eogenesis), predating quartz overgrowths, and again

during late diagenesis (mesogenesis), post-dating quartz overgrowths and chlorite rims. Rutile predominantly appears as framework grains and shows evidence of pedogenic alteration of ilmenite (Fig. 6a), as documented by Pe-Piper et al. (2005).

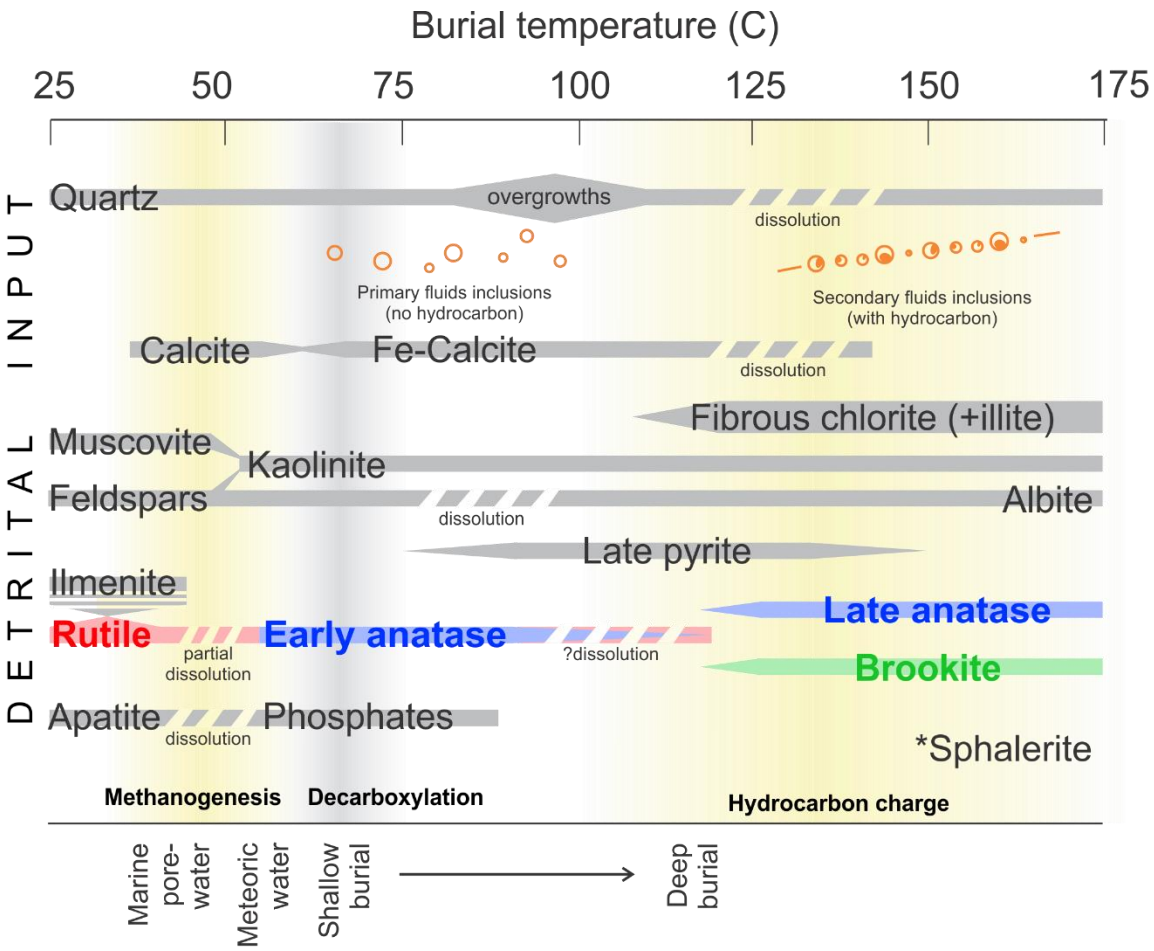

Figure 14. Paragenetic sequence of titania polymorphs (rutile, anatase and brookite) in the Scotian Basin with respect to other minerals and fluid circulation in the basin.

Early mineralization of titania resulted in the precipitation of anatase. The precipitation of early anatase is commonly associated with the partial dissolution of

detrital rutile in the same sample and pseudomorphic replacement of phytodetritus (Figs. 6c and 7f) before sediment compaction and quartz overgrowths. Sponge-like neoformed anatase was also observed on the surface of framework quartz before calcite cementation, hindering the formation of quartz overgrowths (Fig. 8d, yellow arrows indicate quartz overgrowths). The precipitation of anatase before calcite cementation and quartz overgrowths, and the pseudomorphic replacement of uncompacted phytodetritus, suggest replacement or neoformation early in the paragenetic sequence. In previous studies of titania minerals, the precipitation and abundance of early diagenetic titania in samples below sequence boundaries was interpreted as the result of flux of meteoric waters and biogeochemical processes (Pe-Piper et al. 2011).

In most sandstones buried to less than 2.5 km, quartz overgrowths and suturing was not so intensive as to destroy original porosity (Fig. 6b), which is generally filled with Fe-calcite (Fig. 7a), or in some cases with clay minerals (Fig. 7c). The Fe-calcite commonly shows secondary porosity resulting from dissolution (Fig. 7a). Similar cementation of primary porosity is found in some more deeply buried sandstones (Fig. 7f) and primary porosity may be preserved where early chlorite rims on quartz grains inhibited quartz overgrowths (Fig. 7e). Other deeply buried sandstones have been almost totally cemented by quartz suturing and overgrowths and were then pervasively fractured. In some silica-cemented sandstones, fractures and relicts of original porosity experienced widespread dissolution (Fig. 15), which was likely synchronous with the dissolution of Fe-calcite cement in the shallower sandstones. Late titania minerals, chlorite, pyrite,

sphalerite and barite precipitated in these pores and fractures (Fig. 15), although there is no evidence whether all these minerals formed synchronously.

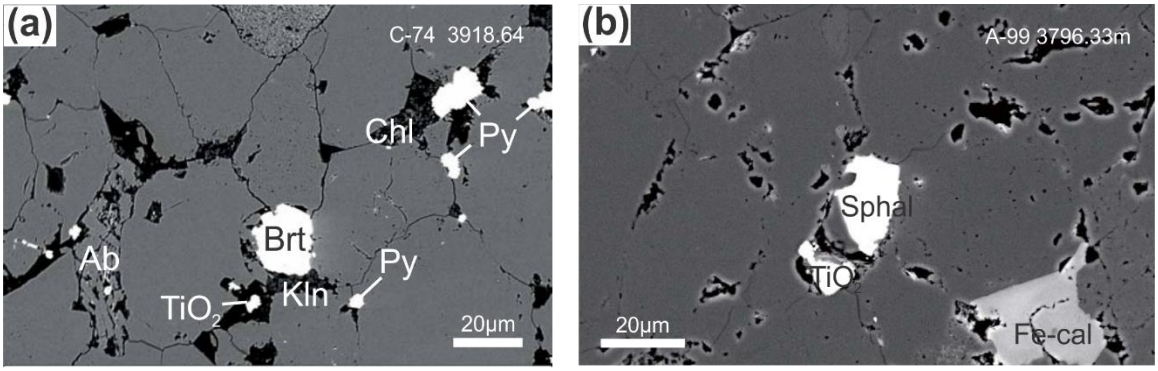

Figure 15. Late titania minerals in fractures. (a) A tiny grain of titania mineral with barite, chlorite and pyrite in fractures. (b) Titania mineral observed with sphalerite in fracture.

The later precipitation of diagenetic titania minerals in the Scotian Basin is associated with the final dissolution of Ti-bearing minerals including the dissolution of early diagenetic titania minerals. Both euhedral crystals of anatase and brookite partially or completely fill pores that display an evident outline of a framework grain (Figs. 7a, 8b and 8c), with brookite post-dating anatase (Fig. 7a, postion a). Brookite engulfs quartz overgrowths (Fig. 7b), and late anatase and brookite both overprint or replace chlorite rims (Figs. 5f; 7e; 7g, position a; and 8e). Secondary porosity resulting from the fracturing and dissolution of quartz also appears to be another important site of late titania precipitation. Rutile, anatase and brookite have all been observed to precipitate in fractures or precipitate as inclusions in quartz crystals where they may fill dissolution voids (Figs. 5d) or replace quartz by a dissolution-reprecipitation mechanism (Fig. 5e). The dissolution of Ti-bearing minerals, such as rutile and dissolution of quartz, suggests either a hot and/or very acidic fluid circulation in the basin at the time. Late diagenetic

sphalerite, which is found in the same fractures as late anatase and brookite, requires high temperatures (~150 °C) and saline fluids for transport and precipitation (Pe-Piper et al. 2015). Secondary fluid inclusions from fractures cutting quartz overgrowths and carbonate cement contain hydrocarbons (Karim et al. 2012) and probably correlate with the fracturing that preceded quartz dissolution.

4.6.2. Titanium solubility in hydrocarbon-rich fluids and halogen-rich brines

Trace concentrations of Ti in crude oil may suggest an ability for hydrocarbon fluids to dissolve Titanium. Ti concentrations in crude petroleum were reported to be between 2–4 ppm (Hardaway et al. 2004) and go up to 11 ppm (Fuchs et al. 2015). The relatively high trace concentrations of Ti in crude oil indicate Ti is soluble in liquid hydrocarbon. An empirical stability index for metalloporphyrin structures, as a means of predicting metal uptake by liquid hydrocarbons, calculated by Fuchs et al. (2015), suggests a solubility for Ti^{4+} (10.2) similar to that of Ni^{2+} (6.8) and V^{2+} (11.05). Nickel and Vanadium are the two most abundant trace metals in crude oils and occur as metalloporphyrins. This indicates that the solubility of Ti in hydrocarbon fluids may be similar to Ni and V, and that hydrocarbon fluid migration in the Scotian Basin was able to transport large amounts of Ti.

Other studies proposed that the presence of halogens (Cl and F) in aqueous solutions increases Ti solubility (Pottier et al. 2001; Schulz et al. 2016; Liu et al. 2019). The highly saline circulating waters in the Scotian Basin aided the dissolution of Ti-bearing minerals by forming Ti-Cl and Ti-F complexes. Another factor to consider is the

presence of Na in solution. Titania solubility is much higher in albite-saturated fluids (Na-Ti(Al)) (Manning et al. 2008) suggesting that precipitation of diagenetic titania may be associated with the dissolution or albitization of K-feldspar (Fig. 2).

4.6.3. Anatase and brookite precipitation

We propose that the mineralization of early diagenetic anatase in the Scotian Basin was facilitated by humic acids released from meteoric waters. Metal-humic complexes are very stable in meteoric waters as dissolved organic matter in natural waters consists of highly oxidized and stable polymeric compounds (Reuters and Perdue, 1977). Chelate Ti-organic complexes caused the mobilization of Ti^{4+} and partial dissolution of Ti-bearing detrital minerals (Fig.16). At a nano-scale, anatase becomes more stable than rutile and even brookite, since anatase formation is dominated by surface energy effects (Reyes-Coronado et al. 2008). Zhang and Banfield (2014) suggested that in natural environments, the stability and growth of titania are mainly controlled by pH. Brookite precipitates under conditions of very low pH while anatase is more stable in higher pH. Therefore, aggregates of anatase will most likely be first to precipitate. In the Scotian Basin, small crystals of anatase are often observed nearby the Ti source. Early diagenetic anatase precipitates along phytodetritus materials or adjacent to a detrital rutile. As pH increases, anatase becomes more stable and may grow larger crystals, as higher pH favours anatase formation and prevents conversion to brookite or rutile. In addition, Ti-F complexes are more stable in low temperatures and pressure and

incorporation of F favours anatase formation. These conditions promote precipitation of anatase, rather than rutile or brookite, during early diagenesis.

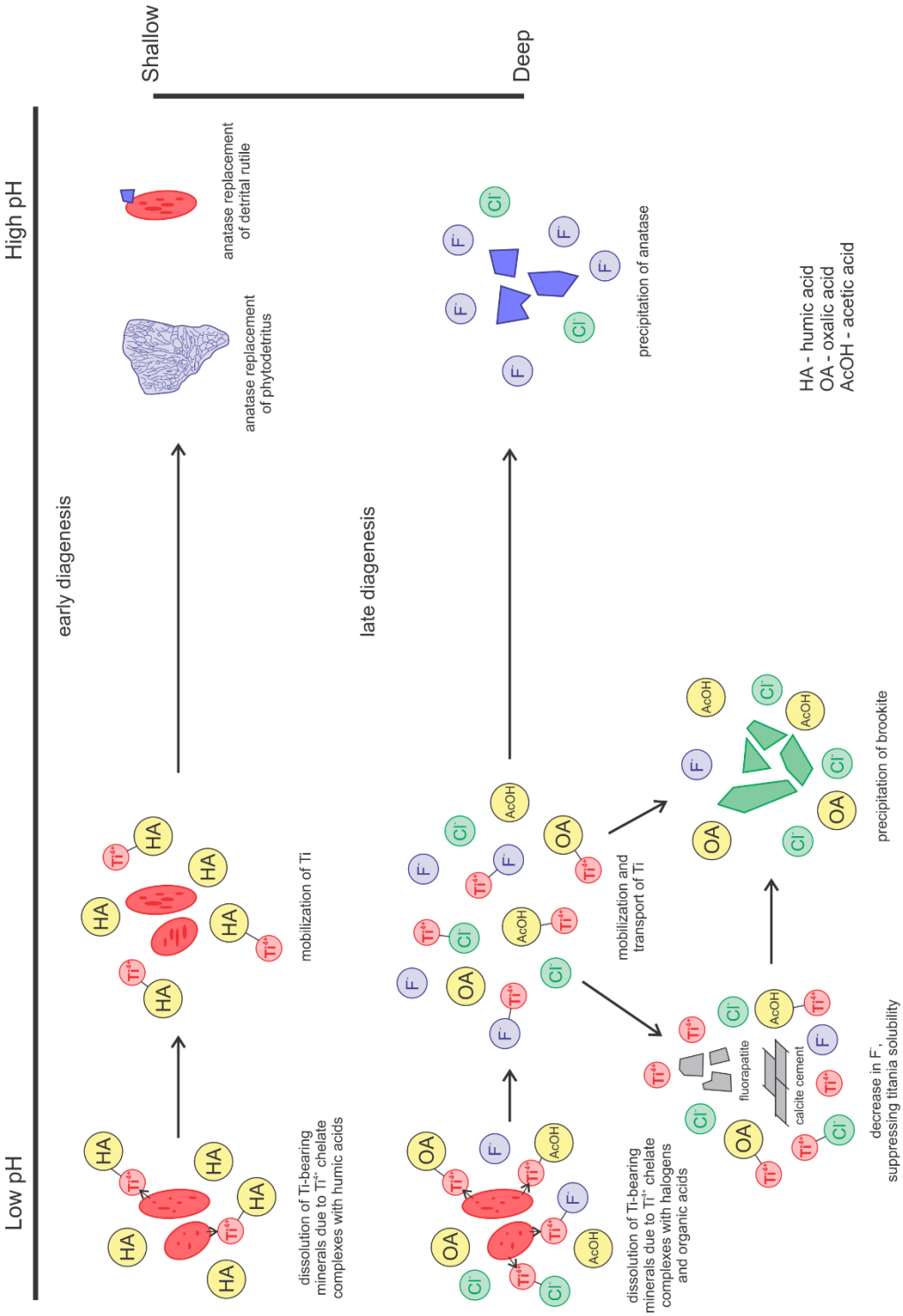

Figure 16. A model of titania precipitation in the Scotian Basin.

The precipitation of late diagenetic anatase and brookite in the reservoir sandstones of the Scotian Basin mostly occurs in secondary cement, suggesting these minerals precipitate in porosity where hydrocarbon fluids flow. We propose that the formation of late anatase and brookite was facilitated by organic acids produced during hydrocarbon generation, aided by the presence of highly saline brines circulating in the system. Similar to humic acids, organic acids (oxalic and acetic) released during hydrocarbon generation and halogens (Cl^- and F^-) from saline brines can form chalate complexes with Ti^{4+} (Schulz et al., 2016; Liu et al., 2019). Geochemistry of diagenetic anatase and brookite from oil/gas producing wells showed relatively high traces of Cl (Fig. 12). The pH condition in this environment would have been low and such complexing would cause detrital Ti-bearing minerals and early diagenetic titania to dissolve. As pH increases, microcrystalline anatase will precipitate. In conditions where the pH stays high, anatase will continue to precipitate. Grains of anatase were observed in samples of low porosity such as Figure 6d. In contrast, in conditions of low pH, aggregates of anatase will convert to brookite and grow as brookite crystals. Formation of brookite and rutile follows a dissolution-precipitation mechanism, where chains of sixfold-coordinated titanium complexes are arranged into different crystal structures (Reyes-Coronado et al. 2008). Brookite is abundant in samples at depths above the free-water level line from Venture, Thebaud and Cohasset fields demonstrating that anatase can easily covert to brookite during crystal growth under conditions that favour brookite formation.

4.6.6. Petroleum significance

Fluids released during mesodiagenesis and hydrocarbon charge facilitated the transport of Ti and later precipitation of titania minerals in the sandstones of the Scotian Basin. Distribution of titania minerals in reservoir sandstones suggests brookite precipitation is synchronous with hydrocarbon charge. The occurrence of mostly brookite above free water lines in Venture, Thebaud and Cohasset fields exhibits the dissolution-precipiation of anatase to brookite under conditions of low pH resulting from the concentration of organic acids in the gas reservoirs.

Further investigation of titania minerals can lead to better understanding of the evolution of hydrocarbon reservoirs. Precipitation of diagenetic titania minerals support evidence that Ti was also mobile in the "wet" wells lacking hydrocarbons reservoirs and that hydrocarbon migration and/or trapping of hydrocarbons was possible. Theoretically, both highly saline brines and hydrocarbons facilitate the dissolution and transport of Ti, and brookite precipitation is favoured by high Cl- abundance. Brookite is predominant even in wells such as Peskowesk A-99 and Louisbourg J-47 lacking highly saline fluids inclusions (Fig. 2). The abundance of brookite rather than anatase may suggest these "wet" potential reservoirs once had hydrocarbon in them. The widespread abundance of brookite and the lack of contrast between anatase and brookite distribution in wells lacking hydrocarbons (e.g. Peskowesk A-99) may suggest escape of hydrocarbons and lack of suitable traps. Whereas in deepwater wells (e.g. Newburn H-23), anatase is rarely detected possibly because of reduced impact of lowstands in allowing flux of meteoric waters during early diagenesis.

4.7. Conclusions

1. In the Mesozoic Scotian Basin, all three common titania polymorphs are present. Rutile is mostly detrital, anatase formed mostly during early diagenesis and brookite is predominantly late diagenetic.

2. Precipitation of early diagenetic anatase is favoured by the presence of early calcite and meteoric water at lowstands of sea level.

3. Ti is mobilized under low pH conditions due to organic acids released during the generation and migration of hydrocarbon-rich fluids in the sediments. Dissolution and transport of Ti is enhanced by the presence of highly saline brines (Argo Salt Formation)

4. Formation of brookite rather than anatase or rutile during late diagenesis may be due to the presence of chloride ions and the incorporation of Fe and V during hydrocarbon charge.

5. The preservation of anatase may be due to less fluid movement related to hydrocarbon charge. Thin sections with less porosity seem to have more anatase than brookite.

6. Titania minerals are important in understanding hydrocarbon migration and accumulation in petroleum sedimentary basins.

Chapter 5: Raman spectra of pseudorutile and kleberite

Abstract

Pseudorutile and kleberite are intermediate minerals formed during alteration of ilmenite to rutile. These alteration minerals are difficult to study as both have a wide range of chemical composition, occur as small sized crystals and are commonly mixed with other minerals. Samples of pseudorutile from three localities (Neptune Island, South Australia; Indonesia; and Scotian Basin, eastern Canada) and loose grains of kleberite sample from Murray Basin, South Australia have been analysed to establish characteristic pseudorutile and kleberite Raman spectra. Raman microspectroscopy offers the possibility of better and quicker mineral identification. Pseudorutile produced a goethite-like Raman spectrum with an increased band shift in the Fe sites. It has characteristic Raman bands with peak positions at 127, 326, 411, 545, 619, and 725–802 cm^{-1} with OH stretching over the interval of 3390–3350 cm^{-1}. Kleberite produced a similar spectrum with a greater Raman shift increase in the Fe sites of the goethite-like band. It has distinctive Raman bands with peak positions at 432, 573, 740, and 820 cm^{-1} and OH stretching at 3390–3350 cm^{-1}. These bands can be used in the future as an easier and quicker method of identifying pseudorutile and kleberite.

5.1. Introduction

Pseudorutile and kleberite are both alteration minerals that form during the alteration of ilmenite to rutile (or anatase) during weathering or diagenesis, and occur in a variety of sedimentary strata. The alteration of ilmenite involves oxidation and leaching

or removal of iron in the presence of water, which results in the production of titania minerals (rutile or anatase) as a residual by-product (Temple, 1966). Frost et al. (1983) used the ratio Ti/(Ti+Fe) to name the mineral phases in altered grains, ilmenite <0.5; pseudorutile 0.5–0.7; leucoxene 0.7–0.9; and rutile >0.9. The presence of pseudorutile as product of ilmenite alteration has been identified in lateritic soils (Anand and Gilkes, 1984), coastal dunes (Puffer and Cousminer, 1982), placer deposits (Schulz and Haser, 2015), and in sandstones in sedimentary basins (Morad and Aldahan, 1986; Grey, 1994; Pe-Piper et al., 2005; Pownceby, 2010). Kleberite has been recognized in Cenozoic sands (Steinike, 2008), and in heavy mineral sand concentrates derived from Murray Basin, southeast Australia (Grey and Li, 2003) and on Kalimantan, Indonesia (Grey et al., 2010).

Pseudorutile is an ilmenite alteration mineral that was first introduced by Teufer and Temple (1966) as a new mineral with an hexagonal symmetry and an ideal composition of $Fe_2^{3+}Ti_3O_9$. However, the Commission on New Minerals and Mineral Names (CNMMN) of the International Mineralogical Association (IMA) did not accept pseudorutile as a valid mineral species. Grey and Reid (1975) refined and determined the crystal structure of pseudorutile using chemical and X-ray diffraction analyses on a single crystal of pseudorutile from Kalimantan, Indonesia. Later, Grey et al. (1994) revalidated pseudorutile as a mineral species assigning Neptune Island, South Australia as the neo-type locality. Another ilmenite alteration mineral, closely related to pseudorutile, was discovered from a confidential uranium exploration project in northeast Germany. This new mineral was first described by Bautsch et al. (1978) and named kleberite without IMA approval. Chemical and X-ray diffraction studies from heavy mineral separates

collected from the Murray Basin, southeast Australia (Grey and Li, 2003) and Kalimantan, Indonesia (Grey et al., 2010) had identified a very similar alteration mineral, referred to as 'hydroxylian pseudorutile'. This mineral produces a similar powder X-ray diffraction pattern as pseudorutile with high content of hydroxyls (Grey and Li, 2003; Grey et al., 2010). Grey et al. (2013) classified 'hydroxylian pseudorutile' as kleberite and re-described its mineral properties using both a kleberite sample from Germany and 'hydroxylian pseudorutile' samples from Australia and Indonesia. As a result, 'hydroxylian pseudorutile' has been accepted as a new mineral by IMA CNMNC and was officially named kleberite, after Dr. Will Kleber.

Although pseudorutile is often described as an oxide mineral in the literature, early Russian studies showed that ilmenite alteration involves hydration/hydroxylation as well as oxidation (Dyadchenko and Khatuntseva, 1960). Later hydrothermal experimental analyses using a synthetic pseudorutile specimen also demonstrated pseudorutile as an oxyhydroxide (Grey et al. 1983). The structure of pseudorutile is based on rutile-goethite intergrowths and can be described as microcrystalline twinned tivanite-type structure ($V^{3+}TiO_3OH$) (Grey and Nickel, 1981). It has a unit cell structure with fine-scale intergrowth of two components: (1) goethite-type M(2)O(OH), and (2) rutile-type $M(1)O_2$. Pseudorutile has dominant Fe^{3+} in the M(2) metal-atom site rather than V^{3+} in tivanite. Kleberite is isostructural with pseudorutile and similarly is a microcrystalline twinned analogue of tivanite-type structure with a dominant Ti^{4+} in the M(2) metal atom site instead of Fe^{3+} in pseudorutile. Chemically, pseudorutile has higher amounts of Fe (35 wt%) and lower amounts of Ti (58 wt%) in comparison to kleberite which has lower

Fe content (11 wt%) and higher Ti content (61-69 wt%). Kleberite has three times more water content and higher contents of SiO_2, Al_2O_3 and P_2O_5 than pseudorutile (Grey et al., 2010).

Previous analytical techniques used for identification were mostly limited to chemical and X-ray diffraction analyses, which require sufficient sample. This study proposes the use of Raman spectroscopy for distinguishing pseudorutile and kleberite from other Fe- and Ti-rich minerals such as goethite, ilmenite, rutile and anatase. Compared to other analytical methods, Raman spectroscopy has the following advantages: (1) it provides positive identification of goethite, ilmenite, rutile and anatase using known Raman spectra of the minerals available in the literature; (2) it is a non-destructive method for Ti-Fe minerals; (3) it has a spatial resolution of approximately 2 microns, ideal for identifying microcrystalline pseudorutile and kleberite.

5.2. Materials and methods

Samples of pseudorutile grains, previously identified by X-ray diffraction and/or chemistry, were studied from three localities. The samples are pseudorutile from Neptune Island, South Australia (Grey et al., 1994; Grey and Li, 2003), Kalimantan, Indonesia (Grey and Reid, 1975), and the Scotian Basin, offshore eastern Canada (Pe-Piper et al., 2005 and unpublished data). In addition, samples of kleberite from Murray Basin, South Australia (Grey et al., 2013) were also analysed to compare Raman spectra with pseudorutile. Loose grains of South Australian pseudorutile, Indonesian pseudorutile and South Australian kleberite were provided by the Commonwealth Scientific and Industrial

Research Organisation (CSIRO), Division of Mineral Resources, Australia. The loose grains were mounted and made into three separate 1-inch epoxy pucks, one for each locality. The pucks were made by placing compression mounting compound powder in a Buehler SimpliMet 1000™ automatic mounting press with a 3-minute bake time at 180 °C and 2100 psi, and an 11-minute cool down. The grains were carefully placed on top of the powder before pressing. The pucks were then polished using diamond paste and were studied under transmitted and reflected light microscope. Five grains with a smooth and flat surface from each sample locality were chosen for this study. In contrast, analysed pseudorutile grains from Scotian Basin are from polished thin sections made from heavy mineral separates of sandstone in the Sable Island 5H-58 well at the 1577.68 m interval. These grains were provided by the Canada-Nova Scotia Offshore Petroleum Board (CNSOPB) Geoscience Research Centre. Mineral grains with the chemical composition of pseudorutile (Frost et al., 1983) were chosen for this study.

All samples were analysed by laser Raman microspectroscopy (Appendix 6-9). Raman spectra were collected using a Horiba Jobin-Yvon LabRam HR confocal instrument, at Saint Mary's University, Halifax, Canada. The equipment uses a 100 mW 532 nm Nd-YAG diode laser from Toptica Phonotics and a Synapse charge-coupled device from Horiba Jobin-Yvon. The reference objective SP-RCO-XP (Horiba Scientific; NIST traceable reference material) was used for frequency calibration. All analyses were acquired using an accumulation of three, 20 second acquisitions at 1% laser power with a 600 grooves/mm grating. The laser has a spot size of approximately 2 µm and a confocal hole diameter of 75 µm. The spectra were differentiated from other Ti-Fe minerals using

known Raman spectra of ilmenite, goethite and rutile referenced from various literature and the RRUFF database. Ilmenite has diagnostic Raman bands at 158, 220, 331, 368 and 687 cm^{-1}. Goethite produces characteristic Raman bands at 223, 240, 298, 386, 397, 477, 548 and 678 cm^{-1} whereas rutile has distinctive Raman bands at 240, 450 and 615 cm^{-1}.

Chemical analyses of South Australian pseudorutile (Appendix 6), Indonesian pseudorutile (Appendix 7) and South Australian kleberite grains (Appendix 8) were also acquired at the Regional Analytical Centre at Saint Mary's University, Halifax, Canada. The analyses were made using a TESCAN MIRA 3 LMU Variable Pressure Schottky Field Emission scanning electron microscope (SEM) equipped with an INCA X-max 80 mm^2 silicon drift detector (SDD) Energy Dispersive Spectrometer (EDS) and Backscattered Electron (BSE) detector. SEM-EDS analyses were used for quick mineral identification whereas BSE images were acquired for textural and morphological details of the studied grains.

Scotian Basin pseudorutile grains were taken for further chemical analysis at the Regional Electron Microprobe Centre at Dalhousie University, Halifax, Canada. Pucks containing pseudorutile samples from South Australia and Indonesia, and a puck with kleberite samples from Murray Basin, were also analysed using the microprobe to compare mineral chemistry of pseudorutile and kleberite to that of Grey et al. (1975) and Grey et al. (2013) respectively. All analyses were performed using JEOL-8200 electron microprobe (EMP) which is equipped with Noran 133 eV dispersive spectrometer and five wavelength spectrometers (WDS). This provides more precise and accurate WDS chemical analyses for the Scotian Basin pseudorutile. The Ti/(Ti+Fe) ratio (Frost et al.,

1986), was calculated using EMP results to distinguish Scotian Basin pseudorutile from other Ti-Fe minerals and/or mixtures such as ‘leucoxene’ (Appendix 9).

5.3. Results

5.3.1 Psuedorutile

The acquired Raman spectra of South Australian and Indonesian pseudorutile over the interval 0 to 2000 cm^{-1} are very similar (Figs 17 and 18). The spectra are consistent with the pseudorutile structure (Grey and Nickel, 1981) and produced a goethite-like band ($3E_g + 2A_{1g}$) and a rutile band ($A_{1g} + B_{1g} + B_{2g} + Eg$) with a complete symmetry of: $B_{1g} + B_{2g} + 4E_g + 3A_{1g}$, with four active modes ($B1_g + 2E_g + A_{1g}$). Nine peaks were assigned with reference to both known goethite and rutile vibrational modes (Table 2). O-H asymmetric stretching vibration was identified around 3390–3550 cm^{-1}. The majority of the peaks (1, 2, 3, 6 and 7-8 in Figs 17-18) at the goethite-like band on both South Australian and Indonesian spectra appears to be shifted to higher wavenumber than those reported in the literature for goethite. Assigned peaks 1 and 4 have a maximum shift of around 11 cm^{-1}. However, it should be noted that a peak assigned to Fe-OH asymmetric stretch at 477 cm^{-1} (peak 4) was only present in one sample, Ind-5. Assigned peak 2 and peak 5 have an increased shift in wavenumber of up to 22 cm^{-1}. Peak 3 has a maximum shift of 32 cm^{-1} whereas peak 7 has a maximum shift of 42 cm^{-1}. The peak assigned at Ti-O in the rutile band remained relatively unchanged.

Table 2. Positions of Raman peaks for pseudorutile and kleberite, values given in cm^{-1}.

Peak no.	Peak assigment as per literature: goethite and rutile*			Pseudorutile			Kleberite
				S. Aus (Ave.)	Ind (Ave.)	Scotian (Ave.)	
1	A1g	Fe-O sym str	223	231	229	220	-
2	Eg	Fe-OH sym bend	298	302	294	290	-
3	Eg	Fe-O-Fe/-OH sym str	397	402	414	412	432
4	A1g	Fe-OH asym str	477	-	488	480	573
5	-	Fe-OH asym str	548	546	549	537	-
6	A1g*	Ti-O*	615*	617	599	610	-
7	-	Fe-O sym str	678	713	701	700	740
8	-	-	-	806	800	810	820

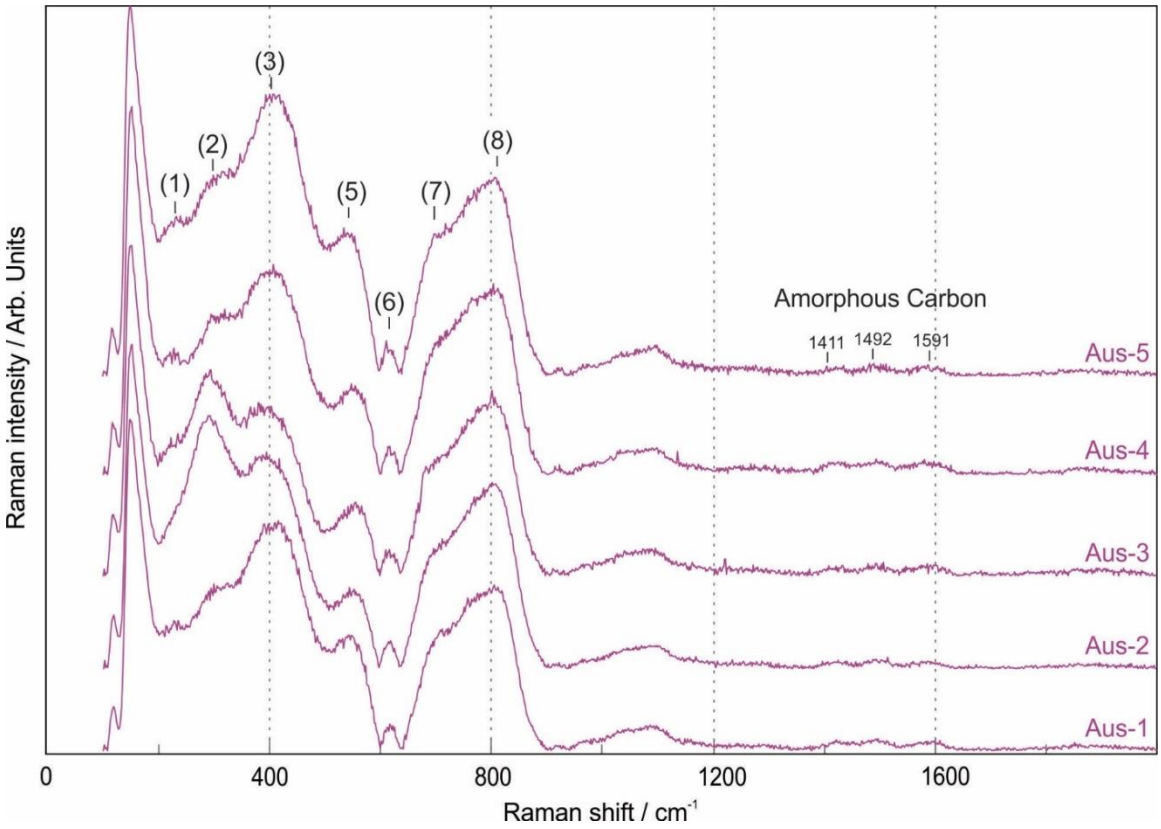

Figure 17. Raman spectra of South Australian pseudorutile showing assigned peak positions.

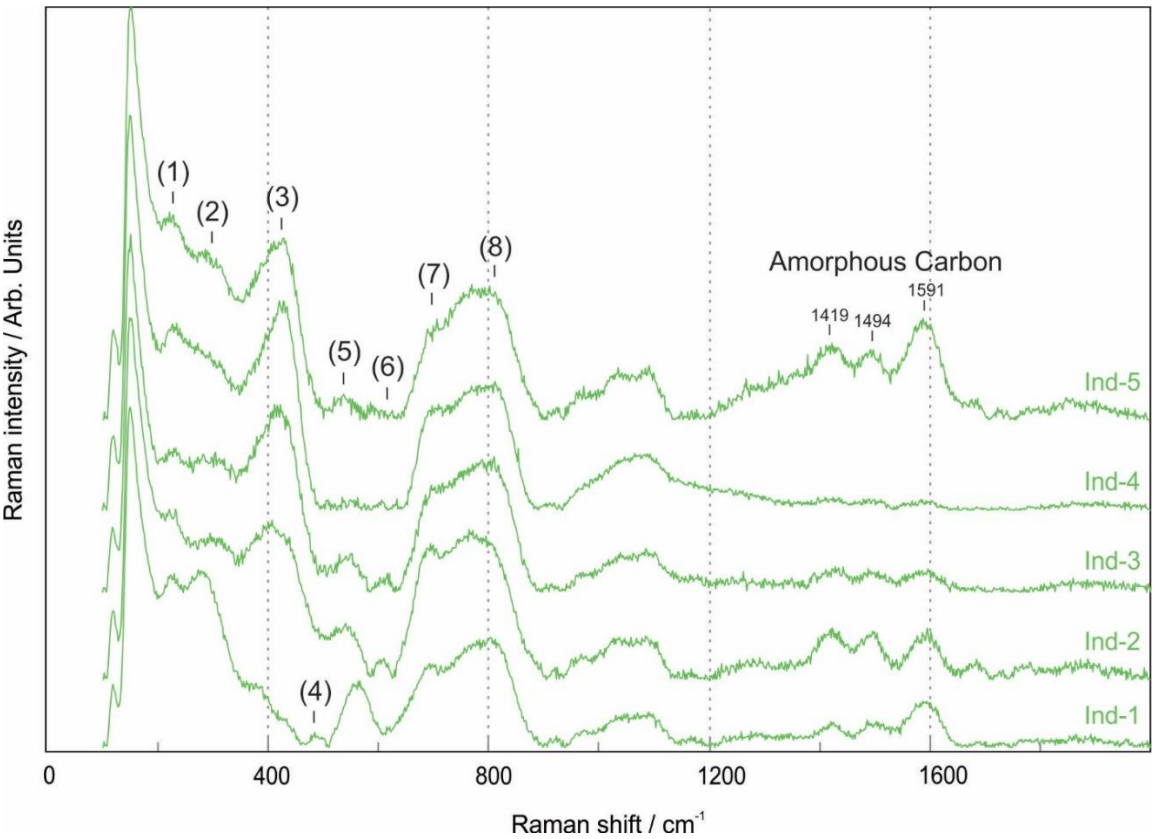

Figure 18. Raman spectra of Indonesian pseudorutile showing assigned peak positions.

Pseudorutile spectra from Scotian Basin also display goethite-like and rutile Raman bands, diagnostic of a pseudorutile structure, but the spectra are mixed with a strong ilmenite band (Fig. 19). Most of the analysed Scotian Basin grains appeared to be mixtures of both pseudorutile and ilmenite. Thus Ti/(Ti+ Fe) calculations (Frost et al., 1986) may not accurately represent pseudorutile if the analyses were from mixtures of ilmenite and pseudorutile. Nevertheless, analyses ordered by Ti/(Ti+Fe) ratio in Figure 3 show systematic variation in Raman band intensity with increasing total Ti/(Ti+Fe).

Amorphous carbon peaks at 1420, 1495 and 1590 cm^{-1} are also more prominent in Scotian Basin samples than elsewhere (Fig. 3).

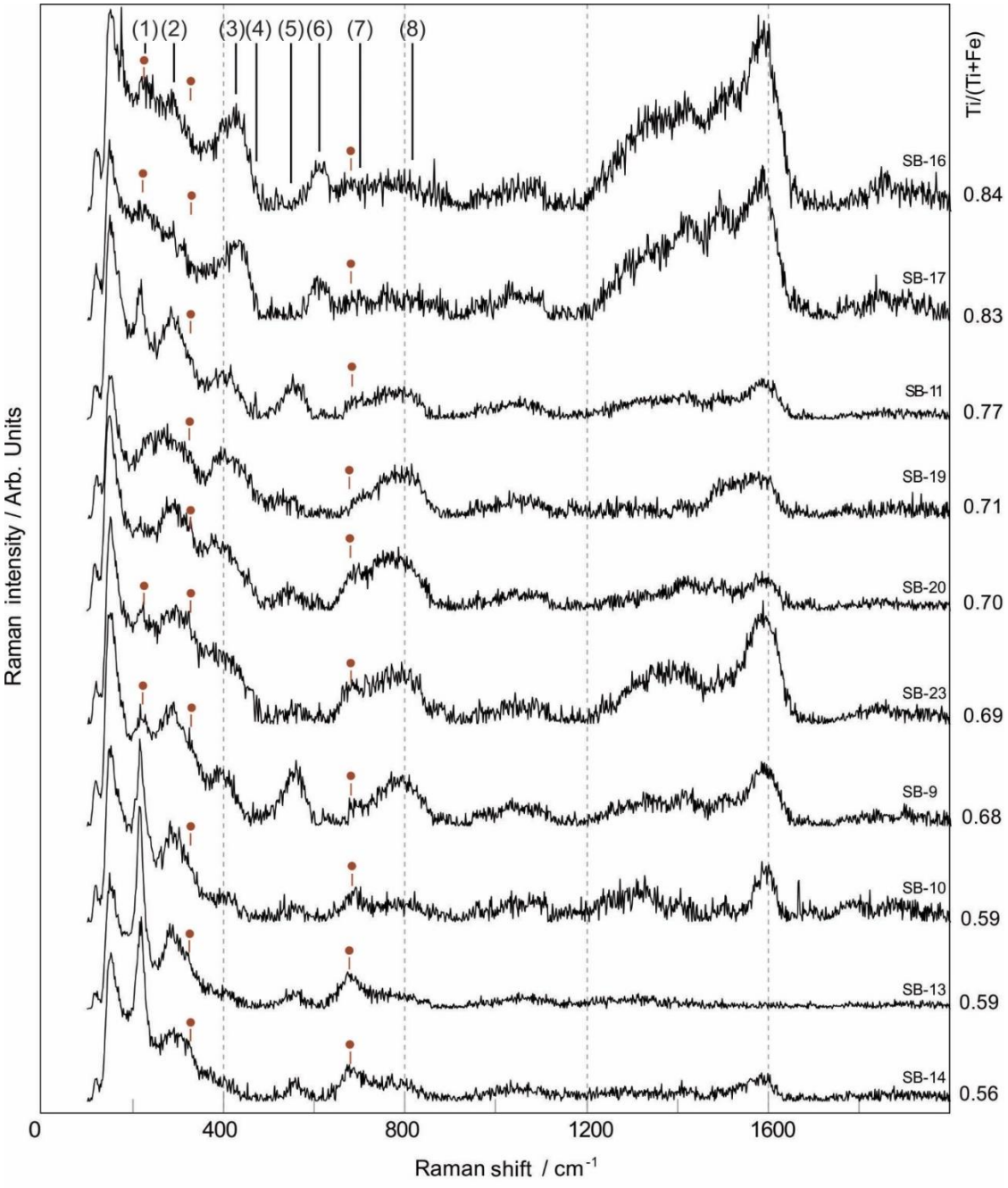

Figure 19. Raman spectra of Scotian Basin pseudorutile arranged based on increasing Ti/(Ti+Fe).

5.3.2. Kleberite

Raman spectra of kleberite over the interval 150 to 2000 cm^{-1} were compared to the spectra of both South Australian and Indonesian pseudorutile (Fig. 20). Although pseudorutile and kleberite are isostructural with elements of goethite and rutile, only five peaks were measured rather than nine peaks observed for pseudorutile. Peaks were assigned with reference to both known goethite and rutile peaks, and the assigned pseudorutile peaks from above (Table 3). O-H stretching is still observed around 3390–3550 cm^{-1} and appears to be more noticeable in kleberite samples compared to pseudorutile samples. The kleberite spectra still display a goethite-like Raman band. However, similar to pseudorutile, the goethite-like band is shifted to greater wavenumber. Assigned peak positions at the Fe-O-Fe/-OH symmetric stretch (peak 1), Fe-OH asymmetric stretch (peak 2), and Fe-O symmetric stretch (peaks 3-4) displayed a Raman shift increase of approximately 30-35 cm^{-1} compared to known goethite peaks, and displayed a shift increase of 21–28 cm^{-1} compared to pseudorutile.

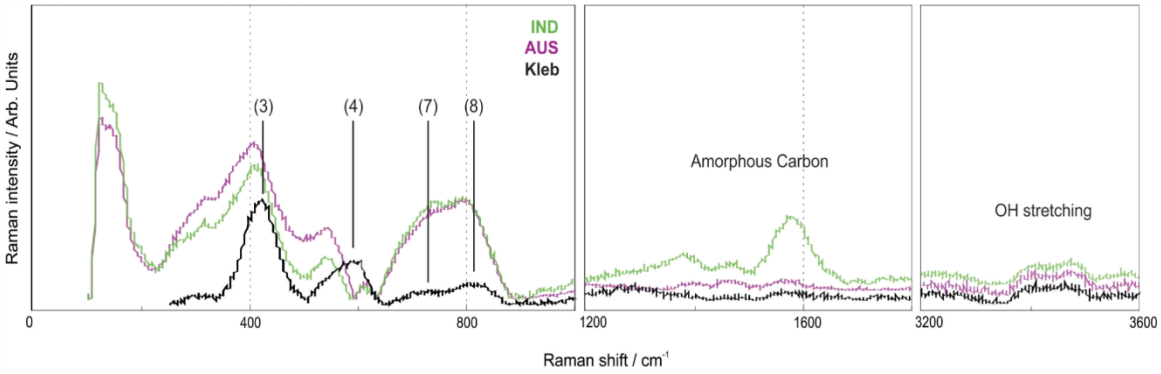

Figure 20. Raman spectrum of kleberite (black) compared to the Raman spectra of South Australian (pink) and Indonesian (green) pseudorutile.

5.4. Discussion

Goethite-like band

The observed Raman shifts from the South Australian and Indonesian samples in the goethite-like band may be due to the substitution of Ti for Fe^{3+} in the goethite-like regions of the pseudorutile structure. A similar study of well-documented shift of vibrational frequencies due to the substitution of Al into goethite shows similar band-shifting to higher wavenumbers (Blanch et al., 2008). The broadening of peak 7 to 8, at 700 to 813 cm^{-1}, may also be due to the substitution of Ti in the Fe^{3+} in the Fe-O symmetric stretching of the goethite-like band as peak broadening can also be a result of element substitution (Blanch et al., 2008). Another consideration is that both pseudorutile samples from South Australia and Indonesia are nanocrystalline (Grey et al. 2010) and powder X-ray diffraction peak widths for the South Australian pseudorutile determined that the anion lattice ordering is confined to regions of about 15 nanometres, and the ordering of the metal atoms (Fe and Ti) is limited to only a few nanometres (Grey and Li, 2003). This nanophase character can have a significant effect on the width, intensity and position of the Raman spectra peaks, compared with more crystalline samples (Sklute et al., 2018).

The Indonesian pseudorutile spectra appear noisier compared to South Australian spectra (Figs 17 and 18). This may be due to the impurities present in Indonesian pseudorutile grains. Previous X-ray diffraction studies showed Indonesian pseudorutile grains to have weak diffraction lines from rutile and ilmenite (Grey and Reid, 1975), whereas South Australian grains were shown to be pure with no reflections of ilmenite

and rutile by X-ray diffraction analyses (Grey, 1994). Thus, the South Australian pseudorutile produces more consistent and clean spectra compared to Indonesian pseudorutile grains.

The increasing Raman shift in the goethite-like band from pseudorutile to kleberite is due to the increase of Ti in the structure. Chemically, kleberite contain higher content of Ti and lower content of Fe compared to pseudorutile. This suggests that higher amount of Ti in kleberite, which resulted in more substitution of Ti in Fe^{3+} goethite-like region in the kleberite crystal structure, resulted in a greater shift in the Raman wavenumber. Chemical analyses of kleberite shows 81-88 wt% Ti, whereas pseudorutile shows a range of 63-73 wt% Ti , with an average 16 wt% Ti difference (Table 3). The Ti substitution may also account to additional broadening of the spectra which masked the rutile Raman band, causing it to be completely inactive.

Table 3. Chemical analyses of pseudorutile and kleberite.

	Pseudorutile							Kleberite	
	South Australia			Indonesia			Scotian Basin	Murray Basin	
	This study SEM (5 grains) average	This study EMP (5 grains) average	(Grey et al. 1975)	This study SEM (5 grains) average	This study EMP (5 grains) average	(Grey et al. 1975)	This study EMP (10 grains) average	This study SEM (5 grains) average	(Grey et al. 2013)
SiO_2		0.22			0.29		0.54	1.4	1.7
TiO_2	65.2	58.01	58.84	69.2	60.42	63.02	63.19	85.2	69.3
Al_2O_3		0.21		0.6	0.4		0.39	1.7	2.5
FeO	33.9	31.86	35.89*	26.7	25.62	30.51*	27.57	10.2	10.30*
Cr_2O_3		0.3			0.2		0.1		
MgO		0.04			0.04		0.09	0.5	0.46
MnO	0.8	0.7	0.6	3.3	2.62	2.87	1.12		0.21
CaO		0.06			0.02		0.03		
Na_2O		0.02			0.03		0.07	0.7	
P_2O_5								0.7	0.41
ZnO		0.03			0.03		0.05		
Nb_2O_5		0.05			0.36		0.06		
BaO		0.03			0.02		0.12		
ZrO_2		0.02			0.03		0.02		
V_2O_5		0.05					0.07	1.4	0.3
H_2O			3.24			2.08			10.9
Total	99.9	91.6	98.57	99.8	90.08	98.48	93.42	100	96.1

Note: all SEM chemical analyses in this study was normalized to 100%, water content was not calculated. FeO* = (FeO + Fe_2O_3). FeO, Fe_2O_3 or (FeO + Fe_2O_3) are recalculated as FeO.

Amorphous carbon

The prominence of carbon peaks at 1420, 1495 and 1590 cm^{-1} in the Indonesian pseudorutile (Fig. 18) may be another form of impurity in the samples. Pseudorutile grains are often porous and are susceptible to impurities. Scotian Basin pseudorutile grains display similar carbon peaks to the Indonesian pseudorutile samples. Although the peaks may be an impurity in the samples. studies in the Venture gas field, 25 km from the Sable Island C-67 well have revealed fluid inclusions of carbon dioxide in silica overgrowths in sandstone (Karim et al., 2011). Other studies have showed that carbon can

be readily absorbed in goethite surfaces under either moist or anhydrous conditions (Russell et al., 1975). The Sable Island C-67 well reported gas and minor light oil (BASIN database https://basin.gdr.nrcan.gc.ca/wells/index_e.php). Thus, the absorption of carbon in the Scotian Basin samples may be related to the petroleum system there.

5.5. Conclusions

The Raman spectrum of pseudorutile includes both goethite-like bands and rutile bands. Pseudorutile can be easily distinguished from other Fe-Ti oxide minerals by using peak positions at 127, 326, 411, 545, 619, and 725-802 cm^{-1} with O-H stretching at 3390-3350 cm^{-1}. The shift to higher wavenumber in the goethite-like band is due to the substitution of Ti for Fe^{3+}. The broadening of the spectra is mainly due to the crystal size effect. Pseudorutile samples from Indonesia and South Australia are nanocrystalline, which affects the width, intensity and even the position of the Raman spectra peaks. Kleberite has a diagnostic Raman spectrum with peak positions at 432, 573, 740 and 820 cm^{-1}. O-H stretching is present at 3390–3350 cm^{-1}. Kleberite clearly shows the increase in the Raman shift is due to the substitution of Ti in the Fe site in the goethite-like band. The presence of amorphous carbon in Scotian Basin pseudorutile samples may be due absorption of carbon dioxide or hydrocarbons.

Chapter 6: Further discussion and outlook

The two chapters presented as draft journal papers represent the work completed within the scope of an M.Sc. thesis. They both take advantage of in-situ Raman analysis to identify titania polymorphs and the mineralogy of alteration products of ilmenite, the principal detrital source of Ti to the Scotian Basin. Chapter 4 documents a paragenetic sequence of titania polymorphs and their relationship to other diagenetic minerals and fluid inclusions. The unexpected observation that in hydrocarbon reservoirs brookite is abundant, whereas anatase dominates below the free water level, can be accounted for by the dissolution-reprecipitation of anatase to brookite under conditions of low pH resulting from concentration of organic acids in the gas reservoirs. Chapter 5 demonstrates the mineralogical complexity of the alteration of ilmenite to rutile, and suggests that earlier interpretations based solely on Fe and Ti content are too simplistic.

The observation of brookite preferentially forming in hydrocarbon reservoirs opens up a whole set of new opportunities and new questions. Can the distribution of anatase vs. brookite be used to assess the evolution of hydrocarbon reservoirs, and in particular can it be used to identify where a reservoir has experienced major leakage? Several factors have been identified that favour the formation of brookite from anatase: not only pH, but also the relative activity of Cl- compared to F-, and the role of trace elements including V. One of the limitations of the present study was the almost complete lack of available inorganic chemical analyses of oil and condensate from the producing fields.

The Scotian Basin is a promising area in which to further investigate some of these questions that are only partially resolved. Ti abundance in the clastic rocks of the basin is unusually high. There are opportunities in the Chaswood Formation (Pe-Piper et al., 2005) and in parts of the basin remote from major fluid fairways to improve the understanding of how detrital ilmenite supplied Ti to the basin. Targeted new sampling of well understood hydrocarbon reservoir systems, such as at the Venture field (Richards et al., 2008) could be used to evaluate hypotheses for controls of anatase and brookite in gas reservoirs. Careful selection of samples from wells lacking hydrocarbons, including focussing on intervals immediately below sequence boundaries, would be useful for further assessment of eodiagenetic titania polymorphs. Obtaining inorganic chemical analyses of oils and concentrates from the various producing fields would allow testing of the hypothesis that trace metals in hydrocarbons influence the chemistry of titania polymorphs.

One limitation of any study is that diagenetic titania minerals are not particularly common. The thin sections analysed in this study represent only about 20% of the available thin sections from each well. The local variability of titania minerals on a decimeter scale is not known.

Chapter 7: Conclusions

1. In the Upper Jurrassic- Lower Cretaceous sandstones of the Scotian Basin, diagenetic rutile is rare, anatase formed mostly during early diagenesis and brookite is predominantly late diagenetic. The precipitation of early diagenetic anatase is favored by the presence of early calcite and low pH meteoric water at lowstands of sea level. Precipitation of late diagenetic titania, principally brookite, is facilitated under low pH conditions due to the presence of hydrocarbon-rich fluids and highly saline brines. Organic acids released from hydrocarbon-rich fluids generated in the sediments further dissolve Ti-bearing detrital minerals (eg. rutile and ilmenite) and eogenetic anatase, by forming organic Ti-complexes. Mobilization and transport of Ti is further enhanced by the presence of highly saline brines. Similar to organic acids, the halogens in the brines can easily form complexes with Ti. Formation of brookite rather than anatase or rutile during late diagenesis may be due to the presence of chloride ions and the incorporation of Fe and V during hydrocarbon charge. The preservation of anatase in low porosity sandstones may be due to less fluid movement related to hydrocarbon charge. The relative abundance of brookite in reservoir sandstones above the free water level suggests that titania minerals are important in understanding hydrocarbon migration and accumulation in petroleum sedimentary basins.

2. Detrital ilmenite supplied to the Scotian Basin alters to pseudorutile and rutile during fluvial transport. Pseudorutile can be distinguished by Raman spectroscopy using peak positions at 127, 326, 411, 545, 619, 725-802 cm^{-1} with O-H stretching at 3390-3350 cm^{-}

[1]. Kleberite has a diagnostic Raman spectrum with peak positions at 432, 573, 740 and 820 cm^{-1}, and O-H stretching is present at 3390–3350 cm^{-1}. The shift to higher wavenumber in the goethite-like band in both spectra is due to the substitution of Ti for Fe^{3+}, while the broadening of the spectra can be attributed to the crystal size effect. Pseudorutile samples from Indonesia and South Australia are nanocrystalline, which affects the width, intensity and even the position of the Raman spectra peaks. Kleberite clearly shows that the increase in the Raman shift is due to the substitution of Ti in the Fe site in the goethite-like band. The presence of amorphous carbon in Scotian Basin pseudorutile samples may be due to the absorption of carbon dioxide or hydrocarbons.

References

Allen, N.S., Mahdjoub, N., Vishnyakov, V., Kelly, P.J. and Kriek, R.J. 2018. The effect of crystalline phase (anatase, brookite and rutile) and size on the photocatalytic activity of calcined polymorphic titanium dioxide (TiO_2). Polymer Degradation and Stability, 150: 31–36. doi:10.1016/j.polymdegradstab.2018.02.008.

Altree-Williams, A., Pring, A., Ngothai, Y. and Brugger, J. 2015. Textural and compositional complexities resulting from coupled dissolution–reprecipitation reactions in geomaterials. Earth-Science Reviews, 150: 628–651.

Arboil, A., Cerda, J., Dezanneau, G., Cirera, A., Piero F., Cornet A. and Morante, J.R. 2002. Effects of Nb doping on the TiO_2 anatase-to-rutile phase transition. Journal of Applied Physics, 92: 853-861.

Anand, R.R. and Gilkes, R.J. 1984. Weathering of ilmenite in a lateritic pallid zone. Clays & Clay Minerals, 32: 363–374.

Barss M. S, Bujak J. P, and Williams G. L. 1979. Palynological zonation and correlation of sixty-seven wells, Eastern Canada. Canada Geological Survey. Paper. 78–25. 117 pp.

Bautsch, H.J., Rohde, G., Sedlacek, P. and Zedler, A. 1978. Kleberit – Ein neues Eisen-Titan-Oxidmineral aus Tertiären Sanden. Zeitschrift für Geologische Wissenschaften, 6: 661-671.

Blanch A.J., Quinton, J. S., Lenehan, C.E. and Pring, A. 2008. The crystal chemistry of Al-bearing goethites: an infrared spectroscopic study. Mineralogical Magazine, 72: 1043-1056.

Bowman, S. J., Pe-Piper, G., Piper, D. J.W., Fensome, R. A. and King, E. L. 2012. Early Cretaceous volcanism in the Scotian Basin. Canadian Journal of Earth Sciences, 49 (12): 1523–1539.

CNMMN (1968) International Mineralogical Association: Commission on new minerals and mineral names.

Canada Nova Scotia Offshore Petroleum Board (CNSOPB) in the 2000 Technical summaries of Scotian Shelf: significant and commercial discoveries.

Canada Nova Scotia Offshore Petroleum Board (CNSOPB) in the 2002 Canada-Nova Scotia Benefits Annual Report for the Sable Offshore Energy Project.

Canada Nova Scotia Offshore Petroleum Board (CNSOPB) in the 2012 Canada-Nova Scotia Benefits Annual Report for the Sable Offshore Energy Project.

Cummings, D.I., and Arnott, R.W.C. 2005. Growth-faulted shelf-margin deltas: a new (but old) play type offshore Nova Scotia: Bulletin of Canadian Petroleum Geology, 53: 211–236.

Cummings, D.I., Hart, B.S. and Arnott, R.W.C. 2006. Sedimentology and stratigraphy of a thick, really extensive fluvial-marine transition, Missisauga Formation, offshore Nova Scotia, and its correlation with shelf margin and slope strata. Bulletin of Canadian Petroleum Geology, 54: 152–174.

Dyadchenko, M. G. and Khatuntseva, A. Y. 1960. Mineralogy and petrology of the weathering process in ilmenite. Dokl. Akad. Nauk SSSR, 132: 435–8.

Frost, M.T., Grey, I.E., Harrowfield, I.R. and Mason, K. 1983. The dependence of alumina and silica contents on the extent of alteration of weathered ilmenites from western Australia. Mineralogical Magazine, 47: 201-208.

Fuchs, S., Schumann, D., Williams-Jones, A.E. and Vali, H. 2015. The growth and concentration of uranium and titanium minerals in hydrocarbons of the Carbon Leader Reef, Witwatersrand Supergroup, South Africa. Chemical Geology, 393–394: 55–66.

Gould, K., Pe-Piper, G. and Piper, D.J.W. 2010. Relationship of diagenetic chlorite rims to depositional facies in Lower Cretaceous reservoir sandstones of the Scotia Basin: Sedimentology, 57: 587–610.

Gould, K. M., Pe-Piper, G. and Piper, D. J. W. 2011. Lateral correlation of sediment facies in the Panuke and Venture fields, Scotian Basin: implications for reservoir connectivity. Geological Survey of Canada, Open File 6838, doi:10.4095/288758

Gould, K. M., Piper, D. J.W. and Pe-Piper, G. 2012. Lateral variation in sandstone lithofacies from conventional core, Scotian Basin: Implications for reservoir quality and conductivity. Canadian Journal of Earth Science, 49: 1478–1503.

Grey, I.E. and Li, C. 2003. Hydroxylian pseudorutile derived from picroilmenite in the Murray Basin, southeastern Australia. Mineralogical Magazine, 67: 733-747.

Grey, I.E. and Nickel, E.H. 1981. Tivanite, a new oxyhydroxide mineral from Western Australia, and its structural relationship to rutile and diaspore. American Mineralogist, 66: 866-871.

Grey, I.E. and Reid A.F. 1975. The structure of pseudorutile and its role in the natural alteration of ilmenite. American Mineralogist, 60: 898-906.

Grey, I.E., Li, C. and Watts, J.A. 1983. Hydrothermal synthesis of goethite-rutile intergrowth structures and their relationship to pseudorutile. American Mineralogist, 68: 981-988.

Grey, I.E., Watts J.A. and Bayliss P. 1994. Mineralogical nomenclature: pseudorutile revalidated and neotype given. Mineralogical Magazine, 58: 597–600.

Grey, I.E., Bordet, P., Wilson, N.C., Townend, R., Bastow, T.J. and Brunelli, M. 2010. A new Al-rich hydroxylian pseudorutile from Kalimantan, Indonesia. American Mineralogist, 95: 161-170.

Grey, I.E., Steinike, K. and MacRae, C.M. 2013. Kleberite, $Fe^{3+}Ti_6O_{11}(OH)_5$, a new ilmenite alteration product, from Konigshain, northeast Germany. Mineralogical Magazine, 77: 45-55.

Hanley, J. J. 2011 The conditions of primary and secondary fluid inclusion entrapment in clastic sedimentary rocks in the Scotian Basin, and the relationship between inclusion entrapment and reservoir charging, in Play fairway analysis atlas: Offshore Nova Scotia: Nova Scotia Department of Energy Report 88-11-00001.

Hughes, Baker, 1999a. Final Well Report to Exxon Mobil for Thebaud 3, available at the Canada-Nova Scotia Offshore Petroleum Board. Geoscience Research Centre.

Hughes, Baker. 1999b. Final Well Report to Exxon Mobil for Thebaud 5, available at the Canada-Nova Scotia Offshore Petroleum Board. Geoscience Research Centre.

Karim, A., Pe-Piper, G. and Piper, D.J.W. 2008, Distribution of diagenetic minerals in Lower Cretaceous sandstones and their relationship to stratigraphy and lithofacies: Glenelg, Thebaud and Chebucto fields, offshore, Scotian basin: Geological Survey of Canada, Open File 5880: 423.

Karim, A., Pe-Piper, G. and Piper, D.J.W. 2010, Controls on diagenesis of Lower Cretaceous reservoir sandstones in the western Sable Subbasin, offshore Nova Scotia: Sedimentary Geology, 224: 65–83.

Karim, A., Pe-Piper, G., Piper, D.J.W. and Hanley, J.J. 2011. Thermal and hydrocarbon-charge history and the relationship between diagenesis and reservoir connectivity: Venture field, offshore Nova Scotia, eastern. Canadian Journal of Earth Sciences, 48: 1293-1306.

Karim, A., Hanley, J.J., Pe-Piper, G., Piper, D.J.W. 2012. Paleohydrogeological and thermal events recorded by fluid inclusions and stable isotopes of diagenetic minerals in Lower Cretaceous sandstones, offshore Nova Scotia, Canada. Bulletin of the American Association of Petroleum Geologists, 96(6): 1147-1169.

Kendell, K. L. 2012. Variations in salt expulsion style within the Sable Canopy Complex, central Scotian margin. Canadian Journal of Earth Sciences, 49(12): 1504-1522.

Larrett, M.J.W. and Spencer, W.G. 1971. Contributions to Australian mineralogy: 3. ‘Pseudorutile’ from South Neptune Island, South Australia. Amdel Bulletin, 12: 74–80.

Ledger, S. 2014. Rutile as an indicator of provenance using texture, morphology and geochemistry and determining the source of sediments for the offshore Scotian Basin. M.Sc. thesis, Saint Mary's University, Halifax, Nova Scotia, 177 pp.

Li, J.G., Ishigaki, T. and Sun, X. 2007. Anatase, Brookite, and Rutile nanocrystals via redox reactions under mild hydrothermal conditions: Phase selective synthesis and physicochemical properties. Journal of Physical Chemistry, 111: 4969-4976.

Li, H., Zhao, G., Chen, Z. and Song, B. 2010. Low temperature synthesis of visible light-driven vanadium doped titania photocatalyst. Journal of colloid and interface science, 344 (2): 247-250.

Liu, Z.R.R., Zhou, M.F., Williams-Jones, A.E., Wang, W. and Gao, J.F. 2019. Diagenetic mobilization of Ti and formation of brookite/anatase in early Cambrian black shales, South China. Chemical Geology, 506: 79–96. doi:10.1016/j.chemgeo.2018.12.022.

Lu, G. and Selloni, A. 2008, Different reactivities of TiO_2 polymorphs: comparative DFT calculations of water and formic acid adsorption at anatase and brookite TiO_2 surfaces: Journal of Physical Chemistry, 112: 6594–6596.

MacLean, B.C. and Wade, J.A. 1993. East Coast Basin Atlas Series: Seismic markers and stratigraphic picks in the Scotian Basin wells. Geological Survey of Canada, East Coast Basin Atlas Series, 276 pp. doi.org/10.4095/221116.

Manning, C., Wilke, M., Schmidt, C., Cauzid, J. 2008. Rutile solubility in albite-H_2O and $Na_2Si_3O_7$-H_2O at high temperatures and pressure by in-situ synchrotron radiation micro-XRF. Earth and Planetary Sciences Letters, 272; 3-4.

Meinhold, G. 2010. Rutile and its application in earth sciences. Journal of Earth-Science reviews, 101 (1-2): 1-28.

Morad, S. and Aldahan, A.A. 1986. Alteration of detrital Fe-Ti oxides in sedimentary rocks. Geological Society of America Bulletin, 97: 567–578.

OETR (Offshore Energy Technical Research Association). 2011. Play Fairway Analysis Atlas - Offshore Nova Scotia. Nova Scotia Department of Energy Report 88-11-0004-01, 349 p. Also available online at http://www.novascotiaoffshore.com/analysis

Okwese, A., Pe-Piper, G. and Piper, D.J.W. 2012. Controls on regional variability in marine pore-water diagenesis below the seafloor in Upper-Lower Cretaceous prodeltaic sandstone and shales, Scotain Basin, Eastern Canada. Marine and Petroleum Geology, 29: 175-191.

Parnell, J. 2004. Titanium mobilization by hydrocarbon fluids related to sill intrusion in a sedimentary sequence, Scotland: Ore Geology Reviews, 24: 155–167.

Parnell, J., Baba, M., Bowden, S. and Muirhead, D. 2017. Subsurface biodegradation of crude oil in a fractured basement reservoir, Shropshire, UK. Journal of the Geological Society, 174. doi:10.1144/jgs2016-129.

Parnell, J., Baba, M. and Bowden, S. 2019. The geochemistry of oil in Cornish granites. Petroleum Geosciences, 25: 298-305.

Pe-Piper, G. and Piper, D. J.W. 2004. The effects of strike-slip motion along the Cobequid-Chedabucto-southwest Grand Banks fault system on the Cretaceous-

Tertiary evolution of Atlantic Canada. Canadian Journal of Earth Sciences, 41(7): 799–808.

Pe-Piper, G., Piper, D.J.W. and Dolansky L. 2005. Alteration of ilmenite in the Cretaceous sandstones of Nova Scotia, southeastern Canada. Clays & Clay Minerals, 53: 490–510.

Pe-Piper, G., Triantafyllidis, S. and Piper, D.J.W. 2008. Geochemical identification of clastic sediment provenance from known sources of similar geology: The Cretaceous Scotian Basin, Canada: Journal of Sedimentary Research, 78: 595–607.

Pe-Piper, G., Karim, A. and Piper, D.J.W. 2011. Authigenesis of Titania Minerals and the Mobility of Ti: New Evidence from Pro-Deltaic Sandstones, Cretaceous Scotian Basin, Canada. Journal of Sedimentary Research, 81: 762–773. doi:10.2110/jsr.2011.63.

Pe-Piper, G. and Piper, D. J. W. 2012. The Impact of Early Cretaceous Deformation on Deposition in the Passive-Margin Scotian Basin, Offshore Eastern Canada, in Tectonics of Sedimentary Basins: Recent Advances (eds C. Busby and A. Azor), John Wiley and Sons, Ltd, Chichester, UK. doi: 10.1002/9781444347166.ch13

Pe-Piper, G., Piper, D. J. W., Zhang, Y. and Chavez, I. 2015. Diagenetic barite and sphalerite in middle Mesozoic sandstones, Scotian Basin, as tracers for basin hydrology. AAPG Bulletin, 99(7): 1281–1313.

Pe-Piper, G., Sangster, C. and Zhang, Y. 2017. Diagenetic F-rich ferroan calcite and zircon in the offshore Scotian Basin, eastern Canada: Significance for

understanding thermal evolution of the basin. American Mineralogist, 102: 1542–1555. doi:10.2138/am-2017-5957.

Pottier, A., Chanéac, C., Tronc, E., Mazerolles, L. and Jolivet, J.P. 2001. Synthesis of brookite TiO_2 nanoparticles by thermolysis of $TiCl^4$ in strongly acidic aqueous media. Journal of Materials Chemistry, 11: 1116–1121. doi:10.1039/b100435m.

Pownceby, M.I. 2010. Alteration and associated impurity element enrichment in detrital ilmenites from the Murray Basin, southeast Australia: a product of multistage alteration. Australian Journal of Earth Sciences, 52: 243-258.

Puffer, J.H. and Cousminer, H.L. 1982. Factors controlling the accumulation of titanium-iron oxide-rich sands in the Cohansey Formation, Lakehurst Area, New Jersey. Economic Geology, 77: 377–391.

Regonini, D., Bowen, C.R., Jaroenworaluck, A. and Stevens, R. 2013. A review of growth and mechanism, structure and crystallinity of anodized TiO_2 nanotubes. Materials Science & Engineering R – Report, 74(12): 377-406.

Reuters, J.H. and Perdue E.M. 1997. Importance of heavy metal-organic matter interaction in natural waters. Geochimica et Cosmochimica Acta, 41: 325-334.

Reyes-Coronado, D., Rodriguez-Gattorno, G., Espinosa-Pesqueira, M.E., Cab, C., Coss, R. and Oskam, G. 2008. Phase-pure TiO_2 nanoparticales: anatase, brookite and rutile. Nanotechnology, 9; 19 (14).

Richards, B., Fairchild, L.H., Vrolijk, P.J. and Hippler, S.J. 2008. Reservoir Connectivity Analysis, Hydrocarbon Distribution, Resource Potential and Production Performance in the Clastic Plays of the Sable Subbasin, Scotian Shelf. Central

Atlantic Conjugate Margins Conference, August 13–15, 2008, Halifax, N.S., Canada. (Extended abstract.) Available for download at http://www.conjugatemargins.com/downloads/publications/Extended%20Abstracts-Revised.pdf

RRUFF database <http://rruff.info/>

Russell, J. D., Paterson, E., Fraser, A. R. and Farmer, V.C. 1975. Adsorption of carbon dioxide on goethite (α-FeOOH) surfaces, and its implications for anion adsorption. Journal of the Chemical Society, Faraday Transactions 1: Physical Chemistry in Condensed Phases, 71: 1623.

Schulz, B. and Haser, S. 2015. The ilmenite – pseudorutile leucoxene alteration sequence in placer deposits in the view of automated SEM mineral liberation analysis. Berlin, Germany, Geoberlin 2015 – abstracts, 338.

Schulz, H.M., Wirth, R. and Schreiber, A. 2016. Nano-crystal formation of TiO_2 polymorphs brookite and anatase due to organic-inorganic rock-fluid interactions. Journal of Sedimentary Research, 86: 59-72.

Sklute, E.C., Kashyap, S., Dyar, M.D., Holden, J.F., Tague, T., Wang, P. and Jaret, S. J. 2018. Spectral and morphological characteristics of synthetic nanophase iron (oxyhydr)oxides. Phys Chem Minerals, 45: 1-26.

Steinike, K. 2008. Der Kleberit im nordöstlichen Teil Deutschlands (1949-1990 Staatsgebiet der DDR). Geohistorische Blätter, 11: 121-128.

Trapalis, C., Todorova, N., Giannakopoulou, T., Romanos, G., Vaimakis, T. and Yu, J. 2008. Preparation of fluorine-doped TiO_2 photocatalysts with controlled crystalline structure. International Journal of Photoenergy, 2008. doi:10.1155/2008/534038.

Temple, A.K. 1966 Alteration of ilmenite. Economic Geology, 61: 695-714.

Teufer, G. and Temple, A.K. 1966. Pseudorutile – a new mineral intermediate between ilmenite and rutile in the alteration of ilmenite. Nature, 211: 179–181.

Triebold, S., Luvizotto, G.L., Tolosana-Delgado, R., Zack, T. and von Eyatten, H. 2011. Discrimination of TiO_2 polymorphs in sedimentary and metamorphic rocks. Contributions to Mineralogy and Petrology, 161: 581-596.

Triebold, S., von Eyatten, H. and Zack, T., 2012. A recipe for the use of rutile in sedimentary provenance analysis. Sedimentary Geology, 282: 268–275.

Wade, J. A. and MacLean, B.C. 1990. Aspects of the geology of the Scotian Basin from recent seismic and well data. Chapter 5. In Geology of the continental margin off eastern Canada. Edited by M.J. Keen and G.L. Williams. Geological Survey of Canada, Ottawa, Ont., Geology of Canada, 2: 190–238.

Whitney, D.L. and Evans, B.W. 2010. Abbreviations fro names of Rock-Forming Minerals. American Mineralogist, 95: 185-187.

Williamson, M.A., 1995. Overpressures and hydrocarbon generation Sable Subbasin, offshore Nova Scotia. Basin Research, 7: 21–34.

Yu, J. C. Ho, W. Yu, J. Hark, S. K. and Lu, K. 2003. Effects of trifluoroacetic acid modification on the surface microstructures and photocatalytic activity of mesoporous TiO_2 thin films. Langmuir, 19 (9): 3889–3896.

Zhang, H.Z. and Banfield, J.F. 2014. Structural characteristics and mechanical and thermodynamic properties of nanocrystalline TiO_2. Chemical Reviews, 114 (19).

Zhang, Y., Pe-Piper, G. and Piper, D. J. W. 2014. Sediment geochemistry as a provenance indicator: unravelling the cryptic signatures of polycyclic sources, climate change, tectonism and volcanism. Sedimentology, 61: 383–410.

Zhang, Y., Pe-Piper, G. and Piper, D.J.W. 2015. How sandstone porosity and permeability vary with diagenetic minerals in the Scotian Basin, offshore eastern Canada: Implications for reservoir quality. Marine and Petroleum Geology, 63: 28-45.